AES/GE/11-03 **Investigation into quantitative visualisation of suffusion**

February 2011 **Esther Rosenbrand**

TU Delft

Department of Geotechnology

Delft University of Technology

Title	:	Investigation into quantitative visualisation of suffusion
Author(s)	:	Esther Rosenbrand
Date	:	February 2011
Professor(s)	:	Prof. dr. M.A. Hicks
Supervisor(s)	:	Dr. Ir. J. Dijkstra Ir. V.M. van Beek (Deltares) Dr. Ir T.J. Heimovaara Dr. Ir. L.A. van Paassen
TA Report number	:	AES/GE/11-03
Postal Address	:	Section for Geo-Engineering Department of Applied Earth Sciences Delft University of Technology P.O. Box 5028 The Netherlands
Telephone	:	(31) 15 2781328 (secretary)
Telefax	:	(31) 15 2781189

Investigation into quantitative visualisation of suffusion

Esther Rosenbrand

February 2011

"Vision is the art of seeing what is invisible to others"

Jonathan Swift

Acknowledgement

I would like express my appreciation to many people for making this an interesting and enjoyable project. To my supervisor Michael Hicks, for giving me the freedom to map out my own course. To Jelke Dijkstra for his guidance, ideas, and many valuable discussions. To all members of my committee, Michael Hicks, Jelke Dijkstra, Vera van Beek, Timo Heimovaara and Leon van Paassen for their input and feedback. To Han de Visser for the practical help in making the experimental setup. To family and friends for providing very welcome distractions and many cups of coffee. I am also grateful to Deltares for providing me with an pleasant working environment these past months.

Esther Rosenbrand

January 2011

Delft University of Technology

Summary

Suffusion is the process whereby seepage water removes fine grains from a soil, which can result in failure of the soil body. This poses a risk for structures founded on soils that are subjected to large hydraulic gradients, such as encountered near hydraulic dams or river levees. Currently, most experimental work on this topic is geared towards quantifying, both the hydraulic gradient at which suffusion initiates, and the flux of eroded material. The reported values vary widely among experiments.

The variation in the results can be explained by taking into account the effect of different experimental conditions. The flux of eroded material is the result of the interplay between particle erosion and filtration within the soil. Visualisation experiments allow for the direct observation of this. The effect of experimental conditions on the individual mechanisms of filtration and erosion, as well as the interaction between these, can be studied. Thereby, visualisation experiments complement methods targeted at quantifying the mass flux leaving the sample.

In this work, the movement of fine grains and the resulting change in the structure of the sample are studied. Common laboratory equipment is used to design a visualisation experiment. The acquired images are analysed using three different quantitative image analysis techniques, with the objective of gaining further insight into the mechanism of suffusion.

Particle image velocimetry (PIV) is an Eulerian method that is applied to determine velocity fields in fluid mechanics and granular flows. During suffusion, the velocity field is discontinuous; fine grains move whilst the coarse grains form a relatively fixed skeleton. This makes PIV less useful for the study of suffusion.

To determine the displacement of individual particles, a Lagrangian method of particle tracking is considered. In the experimental setup used, fine grains are only tracked for a short length of time. This is due to both the large particle displacement between successive images, and the fact that other grains obscure the tracked particles from the camera. These difficulties can be remediated by improvement of the experimental procedure; the former by a higher acquisition rate, and the latter by use of a transparent granular medium where only the tracer particles are visible.

With the apparatus used in this work, the temporal resolution is such that particle displacement cannot be studied unambiguously. Instead, a method of image subtraction (IS) is used that is geared towards quantifying the amount of material that moves. This yields data that can be interpreted to study both how much movement occurs, and where the movement occurs. Furthermore, IS is used to quantify the total change in the structure of the soil sample.

Tests indicate that the load history plays an important role during suffusion. Erosion and filtration cause the soil structure to change, which has a direct effect on further particle transport in the sample. Therefore, the relation between three parameters: the number of moving particles, the location where they move, and the progression of the experiment, is key to understanding the process of suffusion. This is studied by plotting the movement in a 1D section of the sample over time.

It can be concluded that visualisation experiments complement existing outflow experiments to study suffusion. The results of IS can be related to conceptual models that are currently used to describe erosion and filtration processes; these concepts are applicable also to the process of suffusion. Improvement of the experimental setup is required to establish whether the observations reported in this work have a general validity.

Contents

1 Introduction **1**

1.1 Motivation 1

1.2 Objectives 2

2 Suffusion **3**

2.1 Experimental Work 3

2.2 Conceptual Models 5

2.2.1 Filtration 5

2.2.2 Erosion 7

2.2.3 Mass Transport 8

2.3 Role of Visualisation 9

3 Visualisation Experiments **11**

3.1 Mechanical Setup 11

3.2 Image Acquisition 13

3.3 Sample Preparation 14

3.4 Test Procedure 14

3.5 Test Overview 14

4 Image Analysis Using Particle Image Velocimetry **17**

4.1 Method 17

4.2 Application to Suffusion 18

4.3 Evaluation for Suffusion 19

5 Image Analysis Using Particle Tracking **21**

5.1 Method 21

5.2 Application to Suffusion 22

5.3 Evaluation for Suffusion 24

6 Image Analysis Using Image Subtraction **25**
6.1 Related Applications . . . 25
6.2 Method . . . 26
6.3 Application to Suffusion . . . 26
6.3.1 Quantification of Motion . . . 27
6.3.2 Localisation of Motion . . . 32
6.3.3 Evolution of the Sample . . . 36
6.4 Discussion and Evaluation . . . 39
6.4.1 On the Application of IS . . . 39
6.4.2 On the Process of Suffusion . . . 40

7 Conclusions **43**

Bibliography **45**

A Particle Image Velocimetry **49**
A.1 Uniform Displacement . . . 49
A.2 Grayscale Stretching . . . 50

B Particle Tracking **51**
B.1 Tracer Selection . . . 51
B.2 Tracer Identification . . . 52

C Image Subtraction **53**
C.1 Threshold Determination . . . 53
C.2 False Negatives . . . 54
C.3 Quantification of Uncertainty . . . 56

D Data analysis **57**
D.1 Connectivity of Flow Paths . . . 57
D.2 Total Change During Test 7 . . . 57
D.3 High Spatial Resolution IS . . . 59

Chapter 1

Introduction

1.1 Motivation

Erosion of soil by seepage water can lead to a reduction of soil stability with severe consequences. Over half of the historical embankment dam failures can be attributed to seepage erosion [Foster et al., 2000]. Different mechanisms dominate this process; depending on the situation, piping, erosion along discontinuities and suffusion can be distinguished [Richards and Reddy, 2007]. In this work, the removal of fine grains by suffusion is studied. This process occurs in gap graded soils that are internally unstable, as illustrated in Figure 1.1.1. These types of soils are encountered in e.g., natural fluvial deposits [Skempton and Brogan, 1994], and in the cores of hydraulic dams.

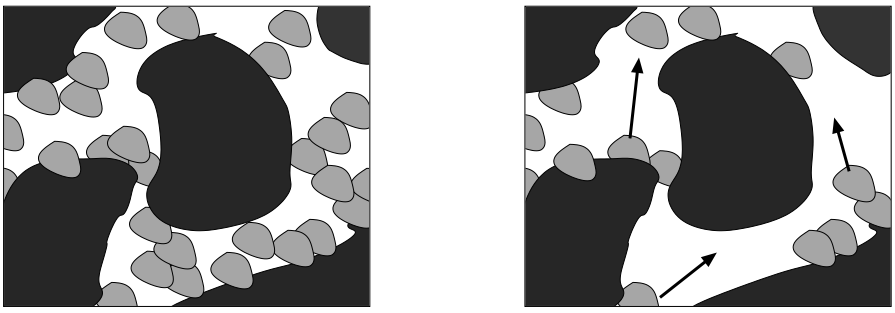

The soil without seepage flow. The pore space is not entirely filled by the fine grains.

Seepage flow mobilises fine grains (particle transport is indicated by arrows).

Figure 1.1.1: A gap graded soil where the fine grains (light) are present in the pore space (white) of the coarse grains (dark).

The fine grains are mobilised by high flow rates. These are induced by extraction wells; in the urban area of Milan this causes concern for the foundations of nearby buildings [Sterpi, 2003]. High flow rates are also encountered in the vicinity of hydraulic dams and river levees. The occurrence of multiple sinkholes in the WAC Bennet Dam [Muir Wood, 2007], for instance, provided a stimulus for increased research in the field of suffusion [Moffat and Fannin, 2006].

Various groups perform laboratory scale experimental work to quantify criteria for the initiation of suffusion: Skempton and Brogan [1994], Fannin and Moffat [2006], Bendahmane et al. [2008], Wan and Fell [2008] and Marot et al. [2009]. The experiments typically involve a modified packed column apparatus, and the amount of fine grains that flows out of the sample is measured. The criteria resulting from these

investigations differ significantly depending on the experimental conditions. To explain these discrepancies, an improved understanding of the physical mechanism of suffusion is required. This is important to develop models that can relate laboratory findings to field situations. Furthermore, models are important to assess the extent to which the soil properties are affected by suffusion, and evaluate what remediation measures can be effective.

Visualisation provides a spatial and temporal resolution that is lacking in outflow experiments [Baumann and Werth, 2004]. This is beneficial to improve the understanding of the processes that occur in the soil. For this reason, visualisation is used to study the filtration of colloids [Ochiai et al., 2006], as well as the mobilisation of particles from a sediment bed [Radice et al., 2006, Papanicolaou et al., 1999].

Quantitative image analysis techniques are required to interpret the data that is obtained from visualisation experiments. Particle image velocimetry (PIV) is used to study the velocity field of e.g., turbulent flows seeded with tracer particles [Cowen and Monismith, 1997, Sveen and Cowen, 2004], and granular flows [Slominski et al., 2007]. Particle tracking (PT), is used to construct the displacement paths of individual particles over a series of images [Crocker and Grier, 1996]. This is often applied to track colloids or bacteria [Gao and Kilfoil, 2009].

To the author's knowledge, current visualisation of suffusion during experimental studies has been limited to qualitative observations made at the sample wall, this is done by e.g., Skempton and Brogan [1994], Fannin and Moffat [2006], Maknoon and Mahdi [2010]. To apply visualisation to the study of suffusion, a suitable method of image analysis and a corresponding experimental setup are required. These are the subject of this work.

1.2 Objectives

The objective of this research is to investigate the possible use of quantitative image analysis techniques for the study of suffusion. An experimental setup will be designed that yields data appropriate to quantitative image analysis. The spatial and temporal scale of the experiment must be sufficient to follow the processes that contribute to the mechanism of suffusion. Literature review, of both experimental and modelling work, is used to identify these processes, and forms the basis for the design of the experiment.

Different image analysis techniques will be considered to study suffusion in a 2D plane strain experiment. During suffusion, a high spatial gradient of the displacement field is inevitable, since the coarse matrix grains are generally immobile and the fine particles are transported. This can lead to a loss of accuracy when PIV is used to determine the velocity field of the sample. However, improvements in computational capacity, have allowed for a significant increase in the spatial and temporal resolution of PIV [Sveen and Cowen, 2004]. In PT, high spatial gradients are not a problem as the displacement of individual particles is of interest. A limitation of this technique is that only a limited number of tracer particles can be studied, which may not be representative for the movement in the entire sample [Radice et al., 2006].

Image subtraction (IS) is commonly applied for motion detection. This method can be applied to the study of suffusion; to quantify the amount of moving particles, as opposed to their velocity or displacement as done in PIV and PT. The resulting data provides scope for different interpretations, and several alternative methods that are particularly suited to the study of suffusion are developed in this work.

The detailed objectives for this study are:

- Design of an experimental setup to enable the visualisation of suffusion.
- Investigation of the possible application of PIV and PT to the study of suffusion.
- Investigation of methods of interpretation of IS data for the study of suffusion.
- Application of IS to the study of suffusion.

Chapter 2

Suffusion

The aim of this Chapter is to investigate the means by which visualisation can contribute to the study of suffusion. The first Section presents an overview of experimental work by those studying suffusion explicitly and those studying closely related phenomena such as filtration and erosion. In the second Section, several currently used conceptual models for suffusion and related processes are considered. In the final Section, the questions that can be addressed using visualisation, and the spatial and temporal resolution that are required for this are summarised.

2.1 Experimental Work

Suffusion is generally studied using permeameter devices. A hydraulic head (or flow rate) is applied to a cylindrical soil sample, that is subjected to a given confining pressure. A similar apparatus is used to study the effectiveness of granular filters for retaining a fine soil, by e.g., Tomlinson and Vaid [2000], Indraratna and Radampola [2002]. The flow rate (or the hydraulic gradient) is measured across -and in experiments by Fannin and Moffat [2006] even within -the sample, and the amount of fines that is present in the effluent is monitored. The results are generally used to determine a critical hydraulic gradient at which suffusion initiates. The values that are reported vary in the range of 0.2 [Skempton and Brogan, 1994] to 168 [Marot et al., 2009].

Different definitions of a critical gradient are in use, e.g., the gradient applied when the first fine particles emerge from the sample [Bendahmane et al., 2008, Wan and Fell, 2008, Marot et al., 2009], or the gradient when the permeability of the sample suddenly rises, which indicates a significant erosion of fines [Tomlinson and Vaid, 2000, Fannin and Moffat, 2006]. This variation in definitions can be one factor contributing to the wide range in the reported critical gradients.

Whether a granular filter or a gap graded soil loses fines due to suffusion depends on the physical space available for particles to be transported, characterised by the the internal stability of the soil, and the hydraulic gradient across, or the flow velocity in, the sample [Tomlinson and Vaid, 2000, Kakuturu and Reddi, 2006]. The shape of the grain size distribution (GSD) curve is commonly used in criteria that predict the internal stability of a soil. The majority of these criteria tend to be conservative, they predict instability for soils that only lose fines when the seepage velocity is extremely high [Wan and Fell, 2008]. Furthermore, different thresholds exist to experimentally classify a soil as internally unstable; a constant rate of loss of fines or a minimum fraction of fines being lost from the sample are commonly reported.

The permeability determines the flow velocity in the soil at a given hydraulic gradient. The flow velocity and not the hydraulic gradient is indicated to be an accurate predictor of suffusion [Reddi et al., 2000, Richards and Reddy, 2007, Bendahmane et al., 2008, Marot et al., 2009]. At higher flow velocities, a greater shear force is exerted by the fluid on the particles, resulting more mobilised grains. The flow velocity can also affect the rate at which suspended particles are filtered [Kakuturu and Reddi, 2006], less particles are retained at higher flow velocities.

The permeability changes as suffusion progresses. Marot et al. [2009] observe a significant decrease in permeability, leading to a reduction in the erosion rate. Reddi et al. [2000] report an initial reduction in permeability, followed by a rise that occurs simultaneously with an increase in the amount of fines that is eroded from the sample. The former test is conducted at a constant hydraulic head; a decrease in the permeability reduces flow velocity and stabilises the soil. The latter test is at a constant flow rate; a reduced permeability results in a build-up of pressure until the blockage is removed.

The porosity of the soil and the confining pressure that is applied are not represented in the GSD curve, but possibly have an important effect on the internal stability and thereby on suffusion [Marot et al., 2009]. Wan and Fell [2008] suggest that loosely packed, more porous soils experience a loss of fines at a lower hydraulic gradient than more densely packed soils.

The volume fraction of the soil that is occupied by the fine grains has a significant effect on suffusion [Marot et al., 2009]. This is attributed partly to the effect on the sample permeability, and thus on the flow velocity. Moreover, Skempton and Brogan [1994] argue that suffusion takes place in soils where the total volume of the fine fraction is less than the volume of the pores in the coarse fraction. Photoelastic tests indicate that stresses are transferred through a granular material by the formation of force networks, whereby some grains are more heavily loaded than others [Drescher and de Josselin de Jong, 1972]. Peters and Berney [2010] find that in gap graded soils, the mechanical behaviour is governed by the coarse fraction when the volume occupied by the fines is less than 40% of the total soil volume. When the intergranular forces are supported mainly by the coarse fraction, the fine grains can be mobilised relatively easily [Skempton and Brogan, 1994].

The rate of increase of the hydraulic head can affect suffusion. Tomlinson and Vaid [2000] suggest that a rapid increase in hydraulic head in filtration experiments allows less time for the fine fraction to form a filter zone that retains the fine particles. Richards and Reddy [2010] are concerned that a rapid increase in the hydraulic head causes a water hammer effect, whereby an increase in pore pressure passes as a wave through the sample.

In experiments where the flow rate is incrementally raised, the interval between the raises may affect the hydraulic gradient at which fine grains are removed from the sample. Tomlinson and Vaid [2000] indicate that intervals of 10 minutes are sufficient to determine if fines are eroded at a given hydraulic head. Moffat and Fannin [2006] report a case where local failure starts after approximately 11 minutes, and the failure zone expands over a period of 15 minutes at a constant hydraulic head. In experiments by Reddi et al. [2000] the mass flux of fines in the effluent stabilises about 20 minutes after the flow rate is increased.

Fannin and Moffat [2006] dissect samples and find cases where erosion is localised in a connected area, a pipe, that forms partly at the sides and partly within the sample. This suggests that preferential flow paths can develop, in which the erosion is concentrated. Even within homogeneously packed columns, the presence of preferential flow is indicated by non ideal solute breakthrough curves [Sugita and Gillham, 1995]. Preferential flow can affect the erosion and the filtration of the fine grains. When more fines are removed in a preferential flow path, this results in an increased porosity and permeability. This positive feedback can play a role in the evolution of preferential flow paths during suffusion.

The study of entrainment of particles from a sediment bed shares many characteristics with the study of suffusion: a mean bed stress is assumed to result in particle mobilisation, there exists a coupling between the bed structure and the flow dynamics, and the threshold that is used to define when the process initiates can vary. The nature of the process requires an accurate physical description [Coleman and Nikora, 2008], which motivates the use of visualisation experiments by e.g., Papanicolaou et al. [1999] and Radice and Ballio [2008].

Visualisation experiments are becoming more commonly used in the study of colloid filtration; for an overview of currently employed methods the reader is referred to Ochiai et al. [2006]. They distinguish between pore scale systems, where only a small number of particles is studied, and core scale systems, where concentrations are studied on the scale of the sample. Results from particle tracking in pore scale tests correspond to particle velocities that are predicted using lattice Boltzmann models [Baumann and Werth, 2004]. To study the effect of heterogeneities and the evolution of preferential flow paths in a sample, core scale studies are recommended [Ochiai et al., 2006].

Permeameter devices allow the boundary conditions to be controlled, and the permeability variation of the sample can be computed throughout the test. A considerable limitation is the difficulty to establish which physical processes result in the observed behaviour. Most of the reported experiments indicate that the flow velocity and the ratio of the size of the pores in the coarse granular skeleton to the size of the fine particles are critical to determine whether suffusion occurs. Many parameters such as the sample porosity, the degree of compaction, and the volume fraction occupied by the fine grains, affect both the pore structure and the flow regime in the sample, making it difficult to asses their overall effect on the mechanism of suffusion. The loading conditions, such as the application of a constant flow rate versus a constant hydraulic head, and the rate at which these are changed during the test must also be considered when comparing measurements from different tests.

In this Section, reasons for the wide variation in the results of the reported suffusion tests are examined. Due to the nature of the process, empirical constants are only valid for specific initial and boundary conditions. In order to relate these values to field situations, it is important to asses the effect of different parameters on the process of suffusion. Visualising the processes of erosion and filtration as they occur can lead to insights that cannot be provided using permeameter tests. These insights, in combination with conceptual models from related fields of study, can complement the current understanding of the process of suffusion.

2.2 Conceptual Models

Models require simplifications and validation using experimental data. Suffusion experiments yield spatially averaged data, favouring volume averaged models in which the amount of material that is removed and the hydraulic gradient are primary variables. Models based on different experimental procedures can give a more detailed treatment of processes that are simplified in suffusion models. As concluded in Section 2.1, an improved mechanistic understanding is beneficial as current empirically determined parameters are only valid for specific boundary conditions.

Three processes, filtration, erosion and mass transport play a significant role during suffusion; models that represent these processes from different areas of study are investigated in this Section. In this context, erosion is considered as the mobilisation of fine particles, and mass transport refers the displacement of both mobilised particles and fluid. The role of visualisation data to support mechanistic suffusion models is discussed in Section 2.3.

2.2.1 Filtration

The process of filtration is underrepresented in many suffusion models; it is awarded greater consideration in the field of colloid transport. Different filtration mechanisms are considered depending on the aspect ratio, $\kappa = {}^{D_{pore}}/_{D_{particle}}$. In situations where $1 < \kappa < 10$ bridging and straining are considered to dominate filtration [Sen and Khilar, 2006]. As illustrated in Figure 2.2.1, bridging occurs when several particles collide and form a bridge blocking a pore; straining occurs when a single particle is too large to pass through a pore constriction.

2.2.1.1 Bridging

A coupled radial model for bridging in a medium with a Gaussian pore size distribution is developed by de Zwart [2007]. The surface forces have a negligible effect on the rate of bridge formation at short timescales. The number of particles that is required to bridge a pore is determined based on the aspect ratio. The flow velocity within each pore, the interstitial velocity, is dependent on the size of the pore. Simulations indicate that more bridges form in the larger pores, due to a higher particle flux there. Increasing the concentration of suspended particles has a strong effect on the amount of bridging. The concentration of suspended particles is a boundary condition in this model, where particle erosion is not considered. Sen and Khilar [2006] suggest that higher flow velocities lead to more erosion and a higher concentration of suspended particles, which can increase the rate of clogging by filtration.

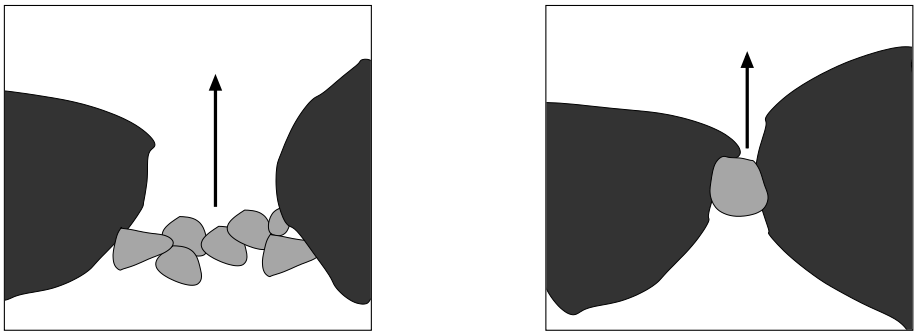

Bridging of the pore constriction by multiple smaller particles.

Straining of a particle that is larger than the pore constriction.

Figure 2.2.1: Filtration mechanisms, the arrows indicate the direction of fluid flow.

2.2.1.2 Straining

Indraratna and Vafai [1997] formulate an analytical model for a base soil-filter system. Fine grains from the base soil can be eroded and trapped in the filter. The filter is represented by a collection of capillary tubes with an equivalent pore size distribution that is derived from the porosity, the GSD and the shape of the filter particles. Within the pores, a base soil particle is subjected to body forces: the gravitational and the buoyancy force, as well as forces acting on its surface: the pressure gradient and friction with the tube wall. The magnitude of the frictional force is determined by the friction angle and the stress normal to the interface, which depends on the horizontal confining pressure on the sample. A limit state equilibrium on the particles is used to determine when particles are filtered, which requires an assumption regarding the mode of transportation of the particles, rolling or sliding. Simulations result in the formation of a sequence of filtration zones where progressively smaller particles are retained. For details and an extension to inclined tubes, the reader is referred to Indraratna and Radampola [2002].

Furthermore, the number of pore necks that each pore is connected to is considered to be important for the process of filtration [Sen and Khilar, 2006]. Locke et al. [2001] extend the model by Indraratna and Vafai [1997] to a 3D pore network model with spherical pores that are connected by pore constrictions. The probability of a particle moving in the direction of fluid flow is determined by considering the possibility of it passing through the different constrictions of the pore. This is used to determine the expected distance that a particle of a given size will travel through the medium.

Shapiro and Bedrikovetsky [2010] present a theory of deep bed filtration on the pore scale, for suspended particles that flow through a filter. This is used to simulate the filtration of an injected pulse of particles, where the particle size as well as the pore size have a stochastic distribution. The particle motion is studied in the framework of continuous time random walks; hereby particles leap from one pore to the next in one time step. Temporal dispersion related to this implementation appears to have a greater effect on the resulting deposition profile than the variations in particle size do.

2.2.1.3 Suffusion Models

In many suffusion models, particle filtration is not explicitly accounted for, e.g., Vardoulakis [2004] and Bucciantini et al. [2010]. A constitutive relation to account for filtration is suggested by Vardoulakis et al. [1996] for a three-phase continuum model, containing a fluid, mobilised solids, and stationary solids. In this relation, filtration is high in areas with a low porosity. The filtration rate increases with the square root of the concentration of mobilised particles and with the flow velocity. However, this relation is not implemented in the model simulations that are presented in the paper [Vardoulakis et al., 1996].

Bonelli and Marot [2008] present a multi-scale model, where erosion and filtration, occurring on the interfaces at the pore scale, are upscaled to macroscale processes. The filtration rate on the interface is

linearly dependent on the concentration of mobilised particles. This relation is similar to a saturation criterion; filtration is assumed to initiate when the concentration of mobilised material exceeds a limit concentration.

2.2.1.4 Conclusion

The processes of bridging and straining are strongly dependent on the pore structure and on the aspect ratio. When the aspect ratio is higher, bridging is the dominant mechanism of filtration. The particle flux, dependent on the suspended particle concentration and the interstitial flow velocity, determines the amount of brigding. The rate of bridging increases with the particle flux due to the increased probability of multiple particles being simultaneously present in a pore constriction. In constitutive relations the suspended particle concentration is also positively correlated to the amount of filtration.

For situations where the aspect ratio is lower, models tend to consider only straining. Both the particle size distribution of the fine grains and the structure of the porous medium determine the amount of straining. The structure of the porous medium is generally described using characteristics from the GSD, the particle shape, and the porosity of the soil; numerical models for this are presented by e.g., Aberg [1992, 1993]. Different representations of the porous medium, as a bundle of tubes e.g., Indraratna and Vafai [1997], Indraratna and Radampola [2002], a pore network e.g., Locke et al. [2001] or a packing of spheres e.g., de Zwart [2007], as well as alternative model implementations result in distinct distributions of filtered particles and a variety of filtration criteria. In constitutive models, the effect of the soil structure on filtration is accounted for implicitly, by relating the filtration rate to porosity e.g., Vardoulakis et al. [1996], or by means of empirically determined constants e.g., Bonelli and Marot [2008].

Mechanistic approaches currently used to model filtration, as well as some constitutive relations that are proposed in the context of suffusion models are discussed here. The filtration models typically neglect the erosion of particles. The amount of particles in suspension is treated as a boundary condition, and particles that are filtered are assumed to remain immobile. During suffusion, the mobilisation of particles plays an important role, and therefore a mechanistic description of erosion is also required.

2.2.2 Erosion

Erosion is important during suffusion as well as in the entrainment of sediment particles in streams. Various models to represent erosion are suggested in literature; these can be classified as those based on a momentum balance on the particle scale, and those using constitutive relations.

2.2.2.1 Momentum balances

A variety of assumptions is made to construct a momentum balance over a particle. One of these regards the geometry of the porous medium as mentioned in the previous Subsection. Alternative representations, such as a capillary tube model e.g., Indraratna and Vafai [1997], or a granular bed with fluid flow above and through it e.g., Coleman and Nikora [2008], result in a different set of forces acting on the grains.

Further assumptions regard the cohesion of the fine fraction; Reddi and Bonala [1997] suggest this can be attributed to a combination of interparticle bonds and mechanical interlocking, whereas cohesion is assumed to be negligible in many other models, e.g., Indraratna and Radampola [2002]. The mode of transport of the particles, by rolling or sliding, furthermore affects the force that is required to mobilise the fine grains.

The fluid drag force is the dominant mobilising force in the momentum balance on the particles. In many models, an average fluid drag force is assumed to act on all particles; the magnitude of this is based on the average rate of fluid flow in the sample, e.g., Indraratna and Vafai [1997] and Bonelli and Marot [2008]. Coleman and Nikora [2008] on the other hand, propose a framework to determine the fluid pressure acting on an individual particle, or a group of particles. This involves a spatial averaging of the fluid pressure over a limited volume, for details the reader is referred to their publication.

2.2.2.2 Constitutive laws

In many multiscale models, erosion is described as an interface process. The erosion rate becomes linearly dependent on the shear stress when this exceeds a critical value, e.g., Bouddour et al. [1996] and Bucciantini et al. [2010]. Bonelli and Marot [2008] model the interface erosion rate as a function of the hydraulic gradient, the porosity and the tortuosity of the soil. The total amount of erosion possible in the latter model is limited, to match experimental findings by Sterpi [2003] where not all the fine material is eroded.

Vardoulakis et al. [1996] present a three-phase continuum model, which is applied by Vardoulakis [2004] to account for the suffusion test results reported by Skempton and Brogan [1994]. The erosion rate is high in areas with a large amount of fines, and is furthermore dependent on the concentration and the flow velocity of the suspended fines, as these exert mobilising forces on the stationary fine grains. Comparable to the model by Bonelli and Marot [2008], not all fines in the sample are eroded. Another relation is suggested by Vardoulakis et al. [2005], which includes an exponential term that reduces the erosion rate to zero when the concentration of suspended fine particles reaches a critical value. Effectively, this includes a filtration effect in the erosion term; but this can only limit the amount of erosion and not account for situations where the rate of filtration exceeds that of erosion.

Le et al. [2010] present an energy analysis for suffusion tests, whereby erosion is accounted for by energy transfer from the fluid to the fine grains. The rate of erosion is related to the temporal derivative of mechanical work, and the total mass eroded to the total energy dissipation. These relations require fitting by experimental data.

In the vicinity of oil wells, internal erosion affects the permeability of the formation. In sand production models, by e.g., Tremblay and Oldakowski [2003] and Papamichos and Vardoulakis [2005], erosion of sand particles is assumed to lead to tensile failure of the sandstone, increasing the erosion rate locally. This positive feedback leads to the formation of an expanding damaged zone in an otherwise homogeneous medium.

2.2.2.3 Conclusion

Constitutive relations, include a factor limiting the total amount of erosion based on experimental data. There is no suggestion regarding the physical process that is responsible for this. Sand production models contain a positive feedback causing erosion to localise. If this also occurs during suffusion, and erosion is limited to the vicinity of distinct flow paths, this could explain why not all fine particles are removed from the soil sample.

Force balances require a number of assumptions regarding the geometry of the porous medium. Additional assumptions regard the fluid forces acting on the particles, and the method of upscaling that is used. It is often assumed that suspended material does not affect the energy balance of the fluid phase, which can lead to strong deviations from the physical situation [Bucciantini et al., 2010]. Models specifically concerned with the transport of suspended solids are addressed in the next Subsection.

2.2.3 Mass Transport

To describe the motion of the fluid phase and the suspended particles, simplifications are needed regarding, e.g., the changing porosity of the porous medium and the suspended particle concentration. Suffusion models tend to treat the fluid phase, as separate from the solid phase, consisting of coarse and fine stationary grains. An alternative approach is to consider the mixture of the entire fine fraction, both moving and stationary particles, and fluid as a granular flow.

2.2.3.1 Suffusion

Fluid transport, in many suffusion models, is treated using a mass balance in combination with a momentum balance where the the concentration of suspended particles is assumed to be low enough to not

influence the properties of the water. Stokes equations are used to determine the interaction between the fluid and the suspended particles, by e.g., Vardoulakis [2004], or the particles are assumed to travel at the same velocity as the fluid, by e.g., Bucciantini et al. [2010]. Locke et al. [2001] account for the effect of the suspended particles on the fluid by increasing the fluid viscosity.

Darcy's law is commonly used to describe the drag force exerted by the solid phase on the fluid phase. Preziosi and Farina [2002] investigate the applicability of Darcy's law in situations where the erosion rate is high. They derive a correction factor, based on thermodynamical considerations, for cases with a high rate of mass exchange between the fluid and the solid phase.

Vardoulakis [2004] models an increase in the porosity of the fine fraction, referred to as an expansion of the fines, using the Richards-Zaki expansion law. This expansion is based on experimental observations by Skempton and Brogan [1994], who report an increase in the permeability of the sample concurrent with fine particles moving about, vibrating in place, at low flow rates. This expansion is only considered during the period where the flow rate is too low to remove the fine particles from the sample.

2.2.3.2 Granular flows

An overview of computational approaches to model the turbulent flow of dispersed particles for industrial applications is given by Portela and Oliemans [2006]. Models for particle tracking allow treatment of the interactions between particles, whereas multi-phase models average the particle behaviour over a phase. The momentum balance for suspended particles in many existing models is based on fluid forces acting on a single particle in an infinite homogeneous medium [Portela and Oliemans, 2006]. This assumption deviates increasingly from reality for higher concentrations of suspended material.

In mixtures with a high concentration of particles, the bulk behaviour is mainly determined by the particle-particle interactions. Ancey and Evesque [2000] present a model for these flows based on force networks in granular media. They distinguish between the particles that carry intergranular stresses, for which particle interactions are mainly frictional, and particles that are not subjected to high stresses that are likely to be involved only in collisional contact with other particles.

2.2.3.3 Conclusion

Granular flows and coupled behaviour between the fluid and the solid phases is complex to model and empirical constants are needed to match experimental data for larger systems [Portela and Oliemans, 2006]. A higher concentration of suspended particles is assumed to exert a greater mobilising force on the fixed solids by Vardoulakis [2004]. This energy transfer is not included in their treatment of the momentum balance of the fluid or the suspended particle phase. Le et al. [2010], on the other hand, directly relate all the momentum that is lost by the fluid phase to the erosion of stationary fine particles.

Suffusion models generally assume a low concentration of mobile particles; yet erosion often occurs for a group of particles [Coleman and Nikora, 2008]. This can lead to temporarily high concentrations of suspended material and a rate of erosion whereby Darcy's law is no longer valid. An alternative approach is to consider the fine fraction as a granular suspension, and treat it in the framework suggested by Ancey and Evesque [2000].

2.3 Role of Visualisation

In this Chapter, various aspects of suffusion have been considered, which has led to the conclusion that the study of suffusion can benefit from the use of visualisation experiments. Constitutive relations and simplified physical descriptions are often justified in the light of the available data. These lead to models that are representative only for specific conditions. Physical descriptions for the separate processes of filtration, erosion and particle transport are available, these can be used as an alternative to the constitutive laws that are applied in the existing suffusion models. This requires a further understanding of the interaction of these processes during suffusion. Visualisation is one method to address this, and

investigate the change in structure of the soil sample, by allowing the direct observation of the evolution of the sample.

One particular aspect of existing suffusion models that can be investigated is the limit on the amount of fine material that can be eroded from the sample. Mobilisation and filtration are strongly linked to the structure and the hydraulic conditions in the porous medium. It is suggested that this coupling can lead to the formation of preferential flow paths that channel the flow, under certain circumstances. Predominantly the fines near the flow paths will be eroded from the sample. Preferential flow can be studied using visualisation experiments that consider the structure of the sample on the core scale.

Visualisation can provide evidence to support either the consideration of erosion as a pure surface phenomenon, or the treatment of the fine fraction as a granular suspension. The expansion of the fine fraction, as suggested by Vardoulakis [2004], can be studied directly. Furthermore, the mode of transport of the particles, in a suspension or by rolling or sliding on the pore walls, can be investigated by studying particle trajectories. This requires a high spatial resolution to enable the study of individual particles.

The disadvantage of studying particle transport using visualisation is that it regards only the particles near the sample wall. There the porosity and the permeability are greater than inside the sample. The objective of this study is to visualise the process in 2D. Differences between the wall and the sample are in the third dimension, but can lead to transport perpendicular to the field of view (FOV). Yoon et al. [2006] visualise colloids to a depth of 3 particle diameters from the wall, and find the behaviour in this region corresponds well with mass balances of the effluent from the sample.

Visualisation provides a spatial and temporal resolution that is lacking in outflow experiments; this is important to support several assumptions made in suffusion models. Specifically in the fields of sediment entrainment and particle filtration, visualisation is increasingly applied to support mechanistic conceptual models. In the field of suffusion this approach is less common, despite the fact that it concerns the same processes of erosion and filtration. For suffusion, visualisation can moreover be useful to study the coupling between erosion and filtration and the sample structure. The tests that are conducted in this work to investigate the potential use of visualisation are described in Chapter 3. The tests are designed to gather data for different methods of quantitative image analysis; the use of PIV, PT, and IS for suffusion is assessed in Chapters 4, 5 and 6 respectively.

Chapter 3

Visualisation Experiments

This work contains an initial investigation of the use of quantitative image analysis for the study of suffusion. In the previous Chapter, questions are raised regarding both particle transport and the evolution of the sample on the core scale. The study of both processes simultaneously presents a challenge regarding the scale of the tests performed. The mechanical setup and image acquisition procedure are selected in an attempt to capture processes occurring both on the particle scale and on the core scale. Modifications to the experimental method, to suit the specific image analysis techniques, are discussed in Chapters 4, 5 and 6. These modifications are constrained to some extent by the available budget.

3.1 Mechanical Setup

The sample is prepared inside a plane strain strongbox consisting of a metal frame containing two glass walls, as shown in Figure 3.1.1. The inside of the box has an area of $400 \times 20\,mm$. To prevent preferential flow at the sides of the sample, a compressible clay coating is applied to the metal frame. From the bottom upwards the model contains: a geotextile, a coarse granular filter ($2.8\,mm \leq D \leq 3.5\,mm$) and a fine granular filter ($1\,mm \leq D \leq 1.7\,mm$). The fine filter causes the flow to spread horizontally in the coarse layer, so that it enters the sample homogeneously. A top load of $3.6\,kPa$, in the form of steel balls of $10\,mm$ diameter, is placed on top of the sample. This allows the fine particles to flow through, and prevents the coarser fraction from being mobilised.

Flow enters the sample through a hole in the bottom of the model and exits through two holes at the sides; this ensures a constant water level above the sample. The capacity of the outlet holes limits the maximum flow rate that can be applied; higher flow rates lead to an overflow. The hydraulic head is supplied by a tank with a constant de-aired water level. The maximum hydraulic head that can be applied is $1.47\,m$; a lower head is applied by partially opening the valve connecting the tank to the sample.

The GSD of the granular material, determined from sieving tests, is shown in Figure 3.1.2. The characteristics of the granular materials are given in Tables 3.1.1 and 3.1.2. D_x is the equivalent grain diameter for which $x\,mass\%$ of the soil has a smaller diameter. The unit weight is determined by measuring the volume of water displaced by a known mass of soil. Porosity is determined by carefully pouring the sample in de-aired water and computing the volume of the water inside the pores. The sample is then compacted by tamping, and the porosity is determined for the tamped soil as well. The volume of the fine fraction is less than the pore space in the coarse fraction, suggesting the intergranular forces acting on the fine particles are negligible.

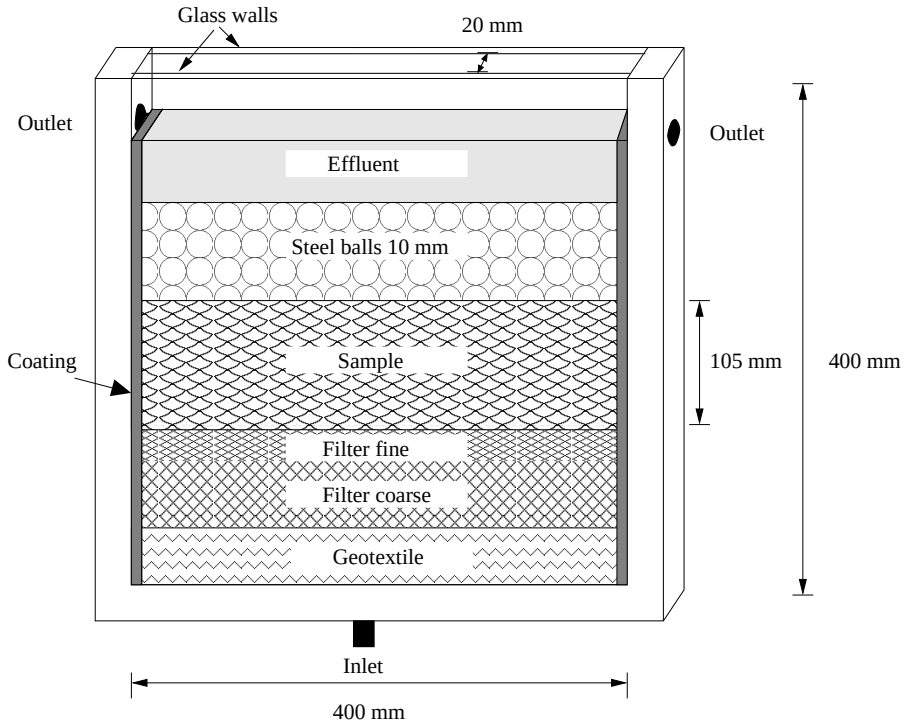

Figure 3.1.1: The strongbox consists of a metal frame with glass sides. Water enters through the inlet and exits through two outlet holes at the sides. The granular filters cause the flow to homogeneously enter the sample. The steel balls prevent the mobilisation of the coarse fraction, but allow the fine fraction to pass through.

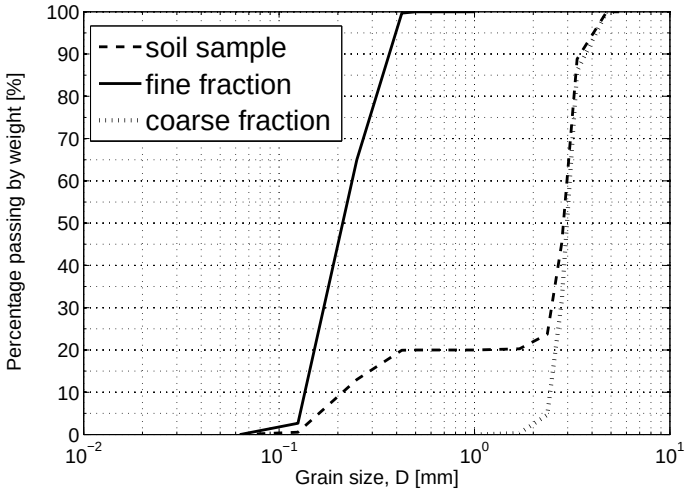

Figure 3.1.2: Grain size distribution curves of the sample and for the fine and coarse fractions.

According to the filter law of Terzaghi et al. [1996], as well as the internal stability criterion of Kenney and Lau [1985], the soil sample used is internally unstable. The filter law predicts that fine grains can move through the filter when $D'_{15}/d_{85} > 4$, where D' refers to the size of the coarse filter particles and d to the size of the fine grains. For the internal stability criterion, the mass fractions of particles with a diameter, $d < D$, and, $D < d < 4D$, are determined, F and H respectively. The soil is internally unstable if (H/F) for any value of D is less than 1 or 1.3, for respectively loose or compacted soils.

Table 3.1.1: Properties of the components.

Properties of components	**Fine**	**Coarse**
Porosity loose [−]	0.37	0.41
Porosity tamped[−]	0.35	0.40
Unit weight $[kNm^{-3}]$	26	26
$D_{50}[mm]$	0.22	3.0
$D_{15}[mm]$	0.16	2.6
$D_{85}[mm]$	0.26	3.4

Table 3.1.2: Properties of the sample.

Properties of sample	
Hydraulic conductivity sample and filter $[cms^{-1}]$	2.2
Initial porosity sample [%]	28
Initial volume sample $[m^3]$ (including pore space)	8.32×10^{-3})
Volume coarse grains $[m^3]$ (solids only)	4.80×10^{-3}
Volume fine grains $[m^3]$ (solids only)	1.20×10^{-3}
Mass coarse $[kg]$	1.28
Mass fine $[kg]$	0.32
$D_{15coarse}/D_{85fine}$	10
$(H/F)_{min}{}^{*}$	0.1

*F is the mass fraction of the sample with $D < 0.5\,mm$, H is the mass fraction with $0.5\,mm < D < 2.0\,mm$.

3.2 Image Acquisition

Images are recorded with a Canon EOS 400D digital single-lens reflex (DSLR) camera (2816×1880 pixels, using 1.38×1.38 binning, sensor size $3.28\,cm^2$). The maximum field of view is $253 \times 169\,mm \approx (84 \times 56)D_{50\,coarse}$. In those images the fine grains are represented by approximately 4 pixels. This allows for the study of individual grains as well as the change in the sample structure on the core scale. Several tests are performed with a smaller FOV, but using the same camera settings, these tests are listed in Table 3.5.1.

A short shutter time is used to capture the particle motion. To reduce the image noise, a low ISO value is used. A large diaphragm opening in combination with illumination from the side by a high energy lamp provides sufficient lighting. Images are saved as normal quality JPEG files; higher quality JPEG or RAW images have no significant effect on the image analysis and decrease the acquisition rate. These camera settings are applied for all tests.

Image acquisition is computer controlled or manual, and images are stored on the camera memory card. Separate images are recorded at a maximum frequency of $1\,fps$ ($frame\,per\,second$), a burst of images is recorded at a frequency of $2.5\,fps$. The latter allows the acquisition of up to 50 images and requires an interval of 2 minutes to store these; no further images can be recorded in this period. The rate of image acquisition is adapted to the experimental conditions; higher rates are used when there is more movement in the sample. Higher acquisition rates are also used when the image analysis method requires a small displacement of particles between successive images.

3.3 Sample Preparation

The sample is prepared by mixing batches of $40\,g$ of fine and $160\,g$ of coarse grains that are moistened to prevent segregation [Skempton and Brogan, 1994]. Tracer particles ($0.6\,g$) are mixed with the fine grains for the tests where particle tracking is investigated. Each batch is manually placed in the strongbox in $1.5\,cm$ of de-aired water, as done by Moffat and Fannin [2006]. To minimise the amount of trapped air, the batches are subdivided into smaller volumes that are individually placed. Each batch is compacted by light tamping. The sample consists of 8 of these batches. Visual inspection indicates that segregation causes a limited loss of fines from the top $1.0 - 1.5\,cm$ of the sample; the remainder of the sample appears homogeneous. The steel balls of the top load are individually placed to avoid disrupting the sample.

3.4 Test Procedure

Image acquisition is started prior to applying the hydraulic head. During the tests, a constant head is applied. A low flow rate, in the order of $0.05 - 0.1\,cms^{-1}$, is applied to the sample for $20\,s$; this causes some rearrangement of fines but no noticeable transport of fines from the sample.

The maximum hydraulic head ($1.47\,m$) is applied by opening the valve of the water tank by 90°. To incrementally increase the hydraulic head, the valve is turned by $30\,^\circ$ at a rate of $\approx 0.3\,^\circ s^{-1}$. Due to interference with image acquisition, the flow rate at each increment of head is measured only after the tests. A float flowmeter (Krohne, NG 60-G10.08, float A III18) is used for flow rates up to $60\,lh^{-1}$, and the effluent volume is measured for higher flow rates. When the valve is opened 30°, 60° and $90\,^\circ$ the respective flow velocities in the sample are $0.2\,cms^{-1}$, $0.4\,cms^{-1}$, and $0.7\,cms^{-1}$. It is assumed that the flow rates during the tests are approximately equal to those measured at the end of the test. Unfortunately, the sample permeability cannot be determined as the hydraulic head is known only over the entire apparatus.

The hydraulic head and the flow velocity in the sample is relatively high, resulting in high Reynolds numbers, $Re = \frac{\rho v d_{30}}{\mu}$, $5 < Re < 19$.

3.5 Test Overview

The aim of these tests is twofold; to investigate suffusion, and to generate images that can be studied using different image analysis techniques. To accomplish this, different flow regimes are applied, and tests are done using a range of spatial and temporal resolutions. Table 3.5.1 gives an overview of the tests that are performed.

The images are analysed using three methods of quantitative image analysis in the following Chapters. For the application of PT, tracer particles are added to the fine fraction in tests 1 through 5. PIV and PT require a limited displacement between successive images. Therefore, these methods are applied only to the images that are taken at the maximum acquisitions rate ($2.5\,fps$). IS is applicable to a wider range of acquisition rates. Manual inspection during the tests plays a significant role in this investigation; the recorded observations are used both to verify the results from image analysis techniques and to evaluate their limitations in the following Chapters.

Table 3.5.1: Test overview.

Test nr.	Test description and hydraulic boundary conditions	Field of view $[mm]$	Acquisition strategy
1	New sample. 2 increments of hydraulic head with $3\,min$ constant head intervals. Stop flow.	140×94	Manual. A burst of images is taken during the application of hydraulic head. After an $\approx 2\,min$ interval to store the data, a second burst is taken during constant head. This is repeated for each increment of head.
2	Continue with sample from test 1. 3 increments of hydraulic head with $3\,min$ constant head intervals. Stop flow.	131×88	As above.
3	Continue with sample from test 2. Same procedure as test 2. Stop flow.	14×10	As above.
4	Continue with sample from test 3. Same procedure as test 2 Stop flow.	14×10	As above.
5	Continue with sample from test 4. Apply first increment of hydraulic head followed by $3\,min$ constant head. Second increment is applied and followed by $7\,min$ constant head. Third increment of hydraulic head is applied and followed by $3\,min$ constant head. Stop flow.	253×169	As above, only with two bursts of images taken during the $7\,min$ constant head.
6	New sample. Application of 3 increments of hydraulic head with $5\,min$ constant head intervals. Stop flow.	103×156	Computer controlled image acquisition. Acquisition rate: $1\,fps$ during application of head increments and first $120\,s$, followed by $0.2\,fps$ during constant head.
7	New sample. Application of 3 increments of hydraulic head with 10 minute constant head intervals.	253×169	Computer controlled image acquisition. Acquisition rate $1\,fps$ during application of head increment and first $15\,s$. Then 25 images at $0.4\,fps$, and 50 images at $0.1\,fps$ until the end of the constant head interval. During closing of valve $1\,fps$.
8	Continue with sample from test 7 without interrupting flow. Flow is applied in cycles, refer to Table 6.3.1.	253×169	Computer controlled image acquisition,$1\,fps$ throughout the test.

Chapter 4

Image Analysis Using Particle Image Velocimetry

In this Chapter, the use of particle image velocimetry (PIV) for the study of suffusion is explored. The method and the algorithm applied in this work are described in Section 4.1; many alternative algorithms exist but these are beyond the scope of this study. In Section 4.2, the limitations of the application of PIV to the study of suffusion are demonstrated. Changes to the experimental method that can improve the applicability of PIV are discussed in Section 4.3.

4.1 Method

PIV is used to determine velocity fields by determining the displacement of material between successive images. This is done by dividing an image into interrogation windows. For each window in the first image, the second image is searched to find a window with a similar appearance. The window from the first image is assumed to move to the location of the matching window in the second image. This is done for all interrogation windows that compose the first image, resulting in a displacement field for the entire FOV. The velocity is determined using the time interval between successive images.

The best size of the interrogation window depends largely on the spatial gradient in the velocity field. All objects that are present inside one interrogation window must have approximately the same displacement; otherwise there is no window with a similar appearance in the second image. During suffusion, the spatial gradient can be high as fine grains move past stationary matrix particles. This requires small interrogation windows, in the order of the size of the moving particles. The minimum size that the interrogation windows can have is limited, however, as a minimum amount of information must be contained within a window. An interrogation window with a low information content can be matched erroneous to multiple windows in the next image; which results in false displacement fields.

Different methods exist to determine the displacement of an interrogation window. Correlation methods are often used; these rely on the covariance function [Sveen and Cowen, 2004]. Gui and Merzkirch [2000] compare cross correlation schemes to the minimum quadratic difference (MQD) algorithm proposed in Gui and Merzkirch [1996]. Particularly for small interrogation windows, the MQD algorithm surpasses classical cross correlation methods with respect to the accuracy of the determined displacement. Therefore the Matlab implementation by Mori and Chang [2003] of that algorithm is applied in this work.

For each interrogation window in the first image, an interrogation window of the same size is moved within a search zone in the second image. The matrices G_1 and G_2 represent the interrogation windows in the first and second image. For each location of the interrogation window in the second image, the quadratic difference between G_1 and G_2 is computed according to Equation 4.1.1, where i and j are the row and column indices, and M and N are the number of rows and columns in the interrogation window. The displacement of G_2 relative to G_1 is given by vector (m, n). The difference function, D, is zero when

the two matrices are identical. The point (m, n) where D has a minimum, therefore, represents the most probable location that the interrogation window has moved to in the interval between the images.

$$D(m,n) = \frac{1}{M.N} \sum_{i=1}^{M} \sum_{j=1}^{N} (G_1(i,j) - G_2(i+m,\ j+n))^2 \tag{4.1.1}$$

4.2 Application to Suffusion

The MQD algorithm is applied to the images resulting from from test 5. The contrast in the fine fraction provides sufficient information to track uniform displacements, as shown in Appendix A.1.

Fine grains are observed to travel large distances, up to $\mathcal{O}(100\,\text{pixels})$, between successive images. This requires a large search zone, making the method computationally expensive. To improve the spatial resolution and minimise the loss of accuracy due to small interrogation windows, multiple regressions of the MQD algorithm are applied. Hereby, the MQD algorithm is applied several times using successively smaller interrogation windows. The displacement that is determined in each step is used to limit the search zone for the following step, in which the length of the interrogation windows is reduced by a half.

An application of the MQD algorithm to two successive images acquired during test 5 shown in Figure 4.2.1. The algorithm is applied in 3 regressions, starting with a window size of 128×128 pixels and ending with 32×32 pixels in the last regression. The black arrows indicate the displacements that are determined, dots indicate that there is little movement. Manual inspection of the original images shows that these displacements are false. When the fines are transported and the matrix remains in place, this causes a change in the content of the interrogation windows. A window with the same content as in the first image, is not present in the second image, and displacement that is indicated does not correspond to the movement of the fine grains.

The minimum value of D, in Equation 4.1.1, for suffusion is significantly higher than the minimum D for a uniform displacement as illustrated in Figure 4.2.2. During uniform displacement, 10% of the search zone has a D value that is lower than the minimum D for suffusion. Thus, 10% of the image area has an appearance that resembles the window in the first image more closely than the best matching window during suffusion. This implies that the minimum value of D is not an accurate measure of the displacement in suffusion images. Manual inspection indicates that the displacements that are determined using PIV do not correspond to the movement of the fine particles. In many cases, even when fine particles are displaced, the interrogation window that indicates no displacement has occurred is most similar to the first interrogation window. This is also seen in Figure 4.2.1, where the dots indicate that no displacement has occurred, and even the largest observed displacement is very small (5 pixels $\approx 0.5\,mm$).

The contrast in the images is improved by rescaling the grayscale range as outlined in Appendix A.2. This results in an increase of the contrast in the fine fraction and a decrease in that of the immobile matrix, so that images resemble those used for fluid dynamics. Unfortunately, this does not improve the PIV results. Pretreatment of the images using Wiener, Gaussian or median filters to remove noise does not significantly affect the displacements that are determined.

Reducing the size of the interrogation windows lowers the minimum value of D; there is less change in the content of the interrogation window. However, as the information content of the interrogation windows is reduced, the windows become less distinct and the range of D values decreases. This increases the probability of a false matching of the interrogation windows. The displacement that is determined using the smaller interrogation windows does not correspond to manually determined displacements.

Application of a different lens, resulting in a FOV of $10 \times 14\,mm$ in tests 3 and 4, results in interrogation windows with an area corresponding to the area occupied by one fine particle. The interrogation windows are not deformed, however, mobilised particles are displaced beyond the FOV.

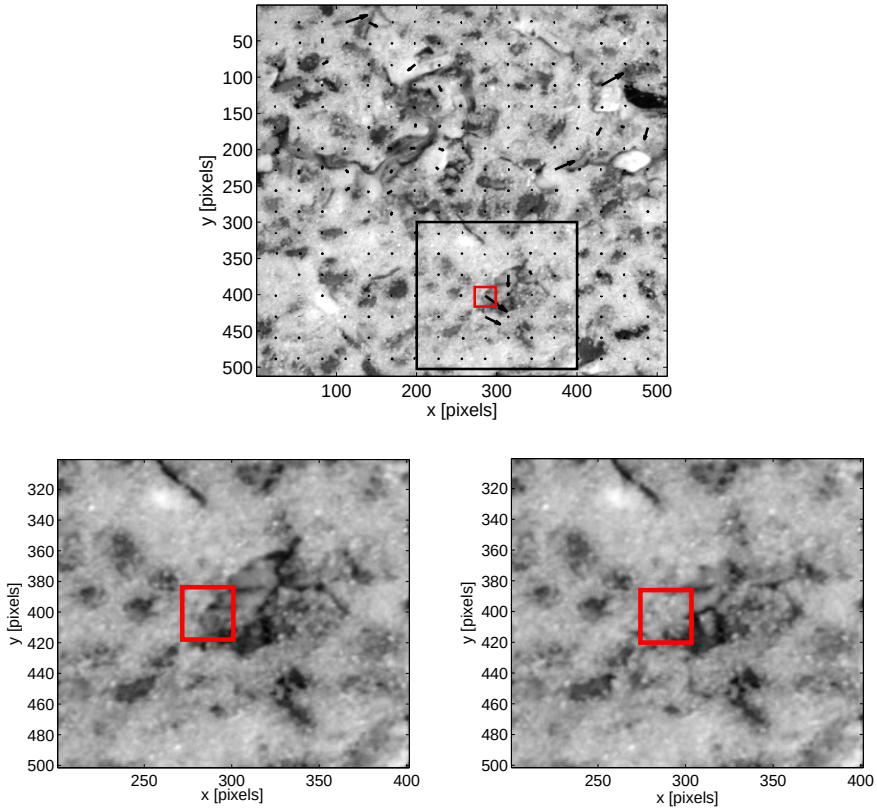

Figure 4.2.1: Top: displacements determined using the MQD algorithm. The initial interrogation window size is 128×128 pixels, and three regressions are performed giving and a final size of 32×32 pixels. The black arrows indicate the displacement. The magnitude of the displacement of the red interrogation window is 5 and 4 pixels in the x and y directions respectively. Bottom: The area indicated by the black rectangle. The location of the red interrogation window in the first image (left) and the location of the window it is matched with in the second image (right). Despite the different appearance of the two windows this combination results in the lowest difference D. $(Scale: 111\,pixels = 10\,mm)$

4.3 Evaluation for Suffusion

PIV, using the images generated in these tests, appears to have limited use for the study of suffusion. The main difference with situations of fluid or granular flow is the presence of a rigid matrix, resulting in a discontinuous velocity field. The internal appearance of the interrogation windows is altered by the transport of fines that neighbour stationary particles. This deformation can be reduced by decreasing the interrogation window length to the size of the fine fraction. However, small interrogation windows contain a low information density, increasing the occurrence of erroneous matches.

Alternative algorithms that account for deformation of the interrogation window can be found in literature, e.g., in the work by Pan et al. [2009]. However, these still require the content of the interrogation window to remain relatively unchanged. High frequency image acquisition is required to minimise the amount of displacement between successive images. This is used in sediment entrainment studies by e.g., Papanicolaou et al. [1999] and Radice et al. [2006]. They study the process for a time length in the order of seconds, and only consider a small number of mobilised grains. The amount of data acquired using the combination of high frequency acquisition and a high spatial resolution makes it computationally expensive to study the process on the core scale for longer periods of time. Therefore, PIV is considered less suitable to analyse the evolution of a soil sample during suffusion in this work. Alternative methods that are less sensitive to high spatial gradients are considered in the next Chapters.

D for two successive image during suffusion.

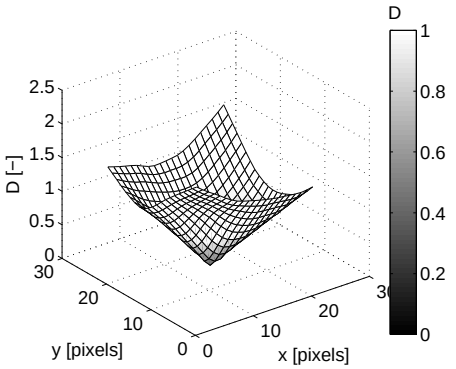

Interrogation window size 64×64 pixels.
$D_{min} = 0.30$

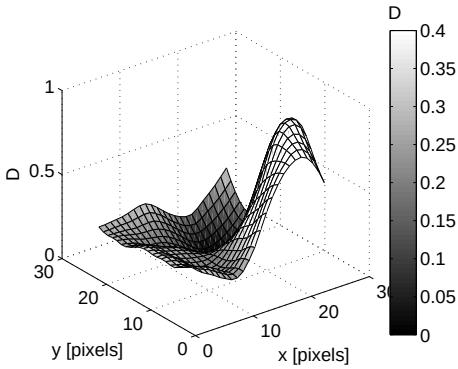

Interrogation window size 16×16 pixels.
$D_{min} = 0.11$

D for a sample image with prescribed displacement.

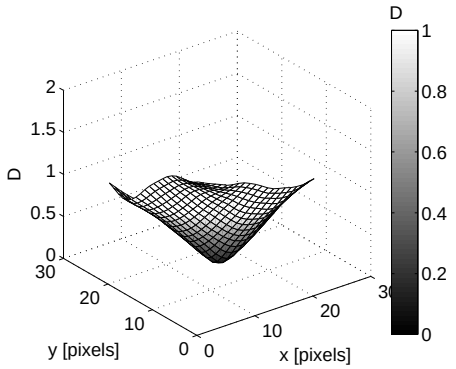

Interrogation window size 64×64 pixels.
$D_{min} = 0.00$
$D < 0.30$ in 10% of the search zone.

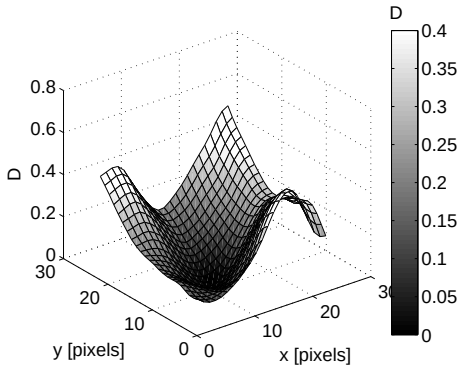

Interrogation window size 16×16 pixels.
$D_{min} = 0.00$
$D < 0.11$ in 10% of the search zone.

Figure 4.2.2: The difference between the content of an interrogation window in the first image and one that is displaced by (m, n) in the second image is given by the difference function, $D(m, n)$. The high D value for the suffusion image pair indicates a significant difference between the appearance of the windows in the two images. During uniform displacement, 10% of the search zone resembles the original window more closely than the best match during suffusion. Smaller interrogation windows result in lower D values, but not in greater accuracy; as the area of the search zone with a value of D that is less than the minimum D in the suffusion images remains 10%.

Chapter 5

Image Analysis Using Particle Tracking

Particle tracking (PT), also referred to as Lagrangian particle tracking (LPT) [Ouellette et al., 2006], is a method whereby the displacement paths of individual particles are reconstructed. Compared to PIV, the accuracy of PT algorithms is less sensitive to high displacement gradients, [Cowen and Monismith, 1997]. PT is performed on images that contain a limited number of tracer particles that are distinct from the background. The location of a particle in successive images is determined, and path is constructed connecting these locations. Methods of locating particles and assigning paths are discussed in the next Section. In Section 5.2 these methods are applied to the images acquired in this work, and the potential use of PT for the study of suffusion is discussed in Section 5.3.

5.1 Method

Crocker and Grier [1996] present a procedure that is widely applied for particle tracking. Implementations of this algorithm for Matlab by Blair and Dufresne [2010] and Kilfoil [2010] are used in this work. The images require pretreatment to remove long wavelength noise, caused by illumination variations, and short wavelength noise, caused by the image acquisition using a DSLR camera. A Gaussian filter is sufficient for the latter. Brightness variations are removed by subtracting the background from the filtered image. The background is modelled by a convolution of the image with a boxcar function with dimensions in the order of the tracer particle size. This combination of operations is equivalent to the application of a bandpass filter.

Particles are the brightest objects in the image, these are distinguished from the background using a threshold value. For all pixels exceeding the threshold, the pixel that has the highest value within an area corresponding to the size of the tracer particles is considered as a particle location [Blair and Dufresne, 2010]. This is to avoid assigning multiple locations to one particle. For spherical particles, the location of the center can be refined by finding the brightness weighted center [Crocker and Grier, 1996].

Tracking requires matching the locations of particles for successive images. Each i^{th} location, x_i^n, in image n, must be linked to a location, x_j^{n+1}, in the next image. To limit the number of possible combinations, a maximum displacement distance, L, is used. The displacement of all particles is determined according to Equation 5.1.1, for all possible tracks. When the number of particles, N, is not the same in consecutive images, the maximum displacement L is assigned to the missing links. The combination that results in the minimum total displacement, d, is considered to be the most probable set of tracks. This method requires the interparticle spacing to be significantly greater than the maximum displacement of a particle between images [Crocker and Grier, 1996].

$$d = \sum_{n} \sum_{i=1}^{N} \sum_{j=1}^{N} \left\| x_j^{n+1} - x_i^n \right\| \tag{5.1.1}$$

To apply PT to suffusion, an appropriate number of distinct tracer particles has to be present in the fine fraction. Initial investigation of different combinations of coarse, fine, and tracer particles indicates that coloured shiny particles can be identified most reliably. Details of the selection can be found in Appendix B.1.

The tracer particles reflect brightly when frontally lit, but appear much darker when they are slightly rotated. They are not identified based on their brightness, but on their colour. In the colour images, each pixel has a red, a green, and a blue (rgb) intensity value. These values are generally added with a standard weighting to obtain a grayscale image. The correlation between the rgb intensities of the tracer particles is significantly different from the rgb correlation for natural soil grains, regardless of the brightness of the tracer particle, as shown in Figure 5.1.1. This correlation is used to establish an alternative weighting, whereby the rgb pixel intensities are added in such a manner that the tracer particles have higher values than both the fine and the coarse grains in the resulting grayscale image. Using this method, however, some coarse grains also have a high value. This requires a second processing step whereby these particles are eliminated based on their size, as detailed in Appendix B.2.

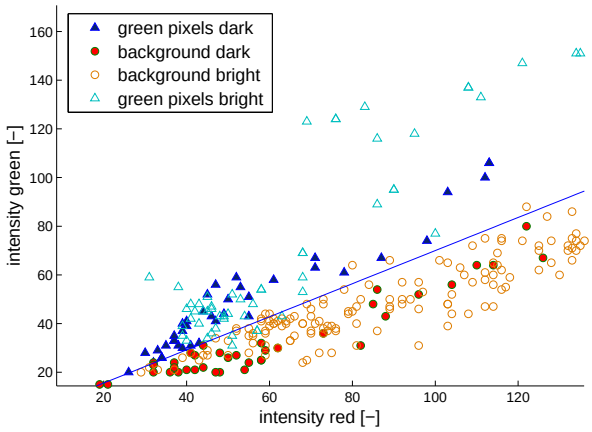

Figure 5.1.1: The green tracer particles are distinguished from the background grains based on the ratio between the green and the red pixel intensities. This distinction works for both the brightly illuminated particles and the darker tracer particles.

In the resulting images the bandpass filter is no longer required, and the particle locating algorithm by Blair and Dufresne [2010] can be directly applied. The threshold value is determined by manual inspection and kept constant throughout the series of images. The refinement, to determine the center of the tracer particles is not performed, as the particles are not spherical.

Due to the large displacement distance, a broad spacing between the tracer particles is required, and only a limited number of tracer particles can be used. This results in a poor representation of the process, as the likelihood that the tracer particles are transported is small. To be able to use a higher seeding density, particles with different colours are used. Different correlations are used to distinguish between these, as detailed in Appendix B.2. A series of images is processed multiple times, tracking one colour each time.

5.2 Application to Suffusion

PT is applied to images from tests 1 through 5. Manual comparison indicates that the methods of particle identification are appropriate to identify all tracer particles without mistaking background regions as particles. An example where green particles are identified is shown in Figure 5.2.1.

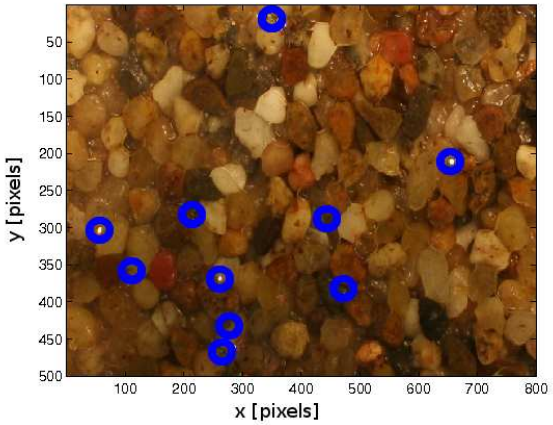

Figure 5.2.1: Identification of green tracer particles. ($Scale: 200\,pixels = 10\,mm$)

Tracking particles presents a greater challenge. The paths that can be assigned to transported particles do not extend beyond three successive images. There are two principle reasons for this that become apparent when zooming in on the sample in tests 3 and 4. Firstly, motion is not strictly two dimensional; mobilised fines obstruct the tracer particle from the FOV, this is illustrated in Figure 5.2.2.

Secondly, large displacements lead to ambiguity concerning the displacement of a particle in the FOV. This is illustrated in Figure 5.2.3, where two green particles are identified in the first image. In the next image, there is only one at a significant distance from the initial particles; in the third image there are again two green particles.

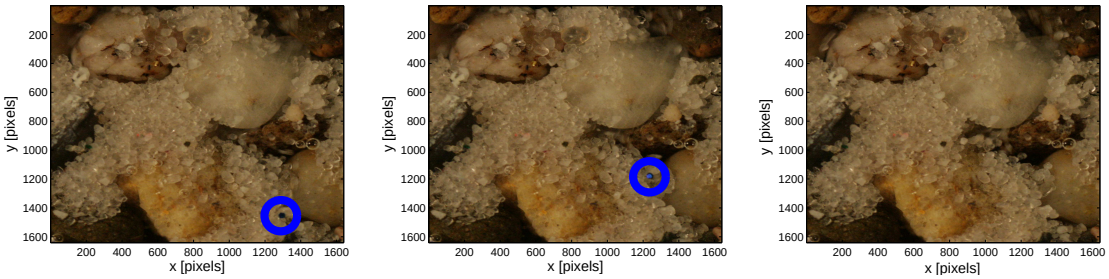

Figure 5.2.2: The blue tracer particle is not apparent in the third image, it is probably concealed by other particles. ($Scale: 201\,pixels = 1\,mm$)

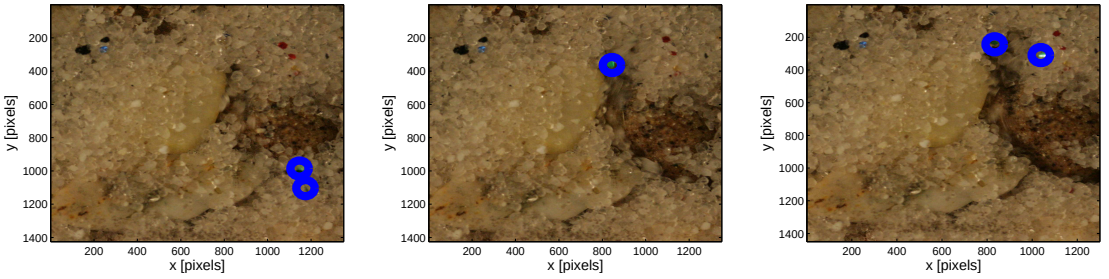

Figure 5.2.3: Large displacements make tracking ambiguous. ($Scale: 201\,pixels = 1\,mm$)

This leads to the fundamental difficulty that even manual determination of paths is ambiguous. It is not possible to make a definite assignment between a tracer particle that is observed in different locations in two images. The possibility that a particle enters the FOV and another one is obscured by moving grains in the interval between two images is a source of uncertainty for many of the tracks that can be constructed.

5.3 Evaluation for Suffusion

The principle difficulty in applying PT to the study of suffusion resides with the ambiguity in assigning tracks. To limit the effect of out of plane motion, micromodels are used for various forms of 2D PT, as outlined by Baumann and Werth [2004]. This reduces the scale of the investigation to the pore level, which is not the objective of this study. An experimental setup, where the coarse and fine fraction as well as the fluid are completely transparent and only tracer particles are visible, is another alternative. This resembles particle tracking in fluids for which 3D PT is commonly applied; for a comparison of various particle locating and tracking algorithms the reader is referred to Ouellette et al. [2006]. In this case, the matrix and fine fraction do not appear in the images, and the coupling between the structure of the sample and the motion of the particles cannot be studied.

In the current setup, only a few tracer particles can be studied as large displacements require a broad interparticle spacing. Increasing the frame rate reduces the distance by which the tracer particles are displaced between images. This allows for a higher seeding density of tracer particles, so that more tracks can be studied. As discussed in the evaluation of PIV, this results in a significant increase in the amount of data, limiting the duration for which the process can be studied. Even using high frequency image acquisition, particle tracks are lost due to clustering of particles [Roarty and Bruno, 2006].

A higher tracer seeding density can also be achieved when applying alternative tracking algorithms. These use knowledge about the displacement field [Cowen and Monismith, 1997], or assumptions regarding the likely change in the velocity or acceleration of the particles [Malik et al., 1993]. Erosion and filtration result in abrupt changes in the movement of particles. Therefore, these alternatives are of less use in the study of suffusion.

PT is a successful method when applied to pore scale models, such as done for bacteria or colloids [Ochiai et al., 2006], or to track particles in 3D, in a transparent model [Ouellette et al., 2006]. For suffusion, the coupling between the structure of the porous medium and the particle motion is of interest. To study this, using the experimental setup designed in Chapter 3, an alternative method of image analysis is more appropriate.

Chapter 6

Image Analysis Using Image Subtraction

The previous Chapters demonstrate that the application of PIV and PT to images acquired in this work is limited, because these methods require the identification of the same particle or group of particles in successive images. In this Chapter, a method based on image subtraction (IS) is considered. This is not based on quantifying the displacement distance, but on quantifying the amount of material that is displaced. The moving particles do not have to be linked between successive images; this makes IS suitable for images in which the displacement is too large for PIV or PT.

Subtracting two grayscale images results in a difference image. This contains zeros where the images are identical, and positive or negative values where an object has moved in the time interval between the two images. Reported applications of IS to the study of erosion or filtration are limited, and treated in Section 6.1. In Section 6.2, the operations used to process difference images in this study are outlined. The method is applied to the study of suffusion in Section 6.3. This leads to a discussion of both the method used and the process studied in Section 6.4.

6.1 Related Applications

Subtraction of images is applied to study the mobilisation of tracer particles in bed load transport. When a particle moves, it appears in the difference image at its initial location as well as at its new location. Keshavarzy and Ball [1999] manually count the number of particles that are displaced in difference images. Radice et al. [2006] show this leads to an underestimation of the amount of mobilised particles, and it is time intensive. Instead, they use image subtraction in combination with PIV, to quantify the number of mobilised particles and determine their velocities. This requires high spatial and temporal resolution for PIV, as elaborated in Chapter 4.

Papanicolaou et al. [1999] use IS for sediment entrainment experiments. They use a very high density of tracer particles. The images are acquired at a high frequency, so that the difference images contain connected particle tracks. This results in difficulties when particles join together in clusters. Due to the high frame rate, the amount of data is so large that a manual evaluation is required to select the sequences of images that will be analysed.

The methods considered above apply IS to track particles between frames, which proves to be problematic for the images used in this study. No applications of IS related to suffusion have been found by this author. The approach suggested in this work makes use of difference images to study how many particles move in a given time interval. The spatial and temporal resolution can be varied to study the movement of individual particles or the evolution of the sample over a longer period of time. The combination of the two yields a large amount of data, which requires a computationally efficient method of data analysis.

6.2 Method

The principle of IS relies on the contrast between the mobile objects and the background; in this case, light fine grains move over darker coarse grains. The difference images have positive values where fine particles are removed, which in this work is referred to as erosion, and negative values where they appear, referred to here as accumulation. The difference images must be processed to minimise false positives, where change is indicated but does not occur, and false negatives where no change is indicated but grains are moving.

False positives can be due to image noise. This results from the experimental setup, and is mainly due to changes in the illumination of the sample. Additionally, there is noise due to image acquisition using a DSLR camera. Application of a threshold to the difference images effectively deals with both types of noise. The appropriate threshold value is determined to minimise the occurrence of false positives. It is important that the chosen threshold value eliminates noise due to variations in lighting intensity throughout the entire test, therefore, the value is determined using samples from the entire sequence of images acquired. The determination of the threshold for tests 7 and 8 is detailed in Appendix C.1.

False negatives are a result of thresholding. The coarse fraction contains a number of light grains. When fines move in front of these, the difference in intensity is below the threshold value. The characteristics of the texture of the image are not sufficient to distinguish between the light coarse grains and the fine fraction, as described in Appendix C.2. To account for movement in areas containing light matrix grains, therefore, an uncertainty margin is added to the measured data. This margin is quantified by manual determination of the fraction of the image area that contains light matrix grains, as described in detail in Appendix C.3.

The magnitude of the value of pixels in the thresholded difference image is not important. To identify whether motion has occurred, all non zero pixels are assigned a value of one. When erosion and accumulation are to be quantified separately, positive and negative pixels are assigned different values. The information that can be obtained from difference images depends on the frame of reference used.

Change can be studied by considering the difference between successive images t_n and t_{n+1} that are separated by a short time interval. Pixels that stand out indicate locations where fine particles are displaced during this interval; these are referred to as areas of motion, or areas displaying activity. Movement also occurs in the path that the particle follows during the time interval, however, this is not apparent in the difference image. Furthermore, the path that particles travel should not be included in a measure of the amount of particles that are mobilised. The length of the time interval between successive images affects the amount of motion that is observed.

Alternatively, the total change can be studied as the difference between an image at a starting time, t_0 and images after a longer time period t_n, t_{n+1}. As opposed to the measure of motion, which quantifies the amount of particles that are mobile during the interval between two images, the measure of total change quantifies the changes in the structure of the sample, which is the result of a succession of movements. The total mass of fines that is eroded and transported out of the sample can be measured independently, and be used to calibrate the measure of total change.

IS, using both perspectives is applied to the images acquired in tests 1, 3 and 6-8. This results in two series of difference images; one for the motion of the fine fraction, and one for the evolution of the sample over longer time intervals. Methods of data interpretation based on these difference images are presented in the following Section.

6.3 Application to Suffusion

The application of PIV and PT analyses, in combination with manual inspection, yields qualitative information about the mechanisms that occur during suffusion. Particle motion is characterised by a series of sizable leaps, separated by time intervals when the particle is at rest. More motion occurs when the hydraulic head is increased than during periods of constant flow. The sample tends to develop areas through which fines are transported for a longer period of time, preferential flow paths, whilst there is

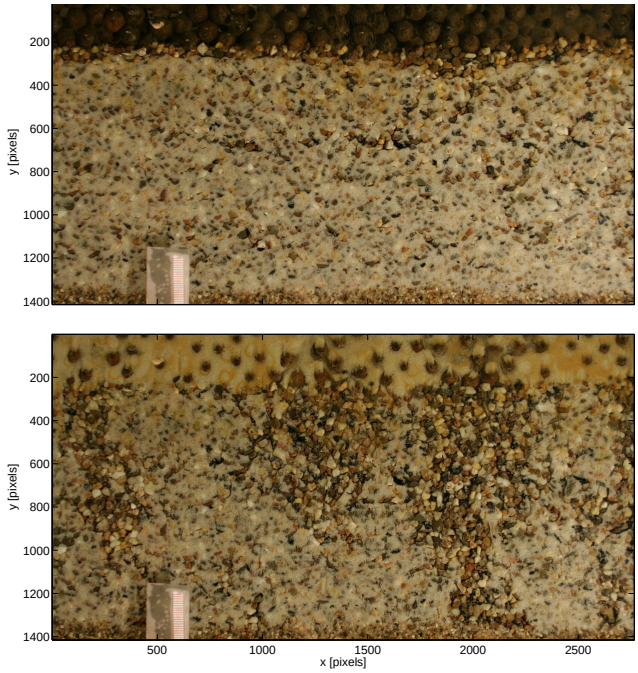

Figure 6.3.1: State of sample at the start (top) and at the end (bottom) of test 7. The sample is present between $y-$coordinates 220 and 1380. ($Scale: 111\,pixels = 10\,mm$)

little to no motion in the rest of the sample. Most erosion is localised in specific areas that become depleted of fines, whereas in other areas there is little mobilisation at all, as shown in Figure 6.3.1.

In this Section, these observations are quantified using IS. In Subsection 6.3.1 the area indicating change in the difference images is determined, yielding spatially averaged information regarding motion and total change in the appearance of the sample relative to the progression of the test. In Subsection 6.3.2 the data is interpreted within its spatial context. A third option is to visualise the activity in a vertical section of the sample for the duration of the test, as done in Subsection 6.3.3.

6.3.1 Quantification of Motion

The amount of motion is quantified by a summation of all pixels that indicate erosion and accumulation in one difference image. This value is scaled by the total number of pixels in the image. As discussed in the previous Subsection, some areas of the matrix have a low contrast with respect to the fine fraction leading to uncertainty in the measured amount of motion. Given that the light matrix grains are distributed randomly throughout the sample, the assumption can be made that the frequency with which fine grains move over these grains, is the same as the frequency with which they move over other sections of the image. The uncertainty margin that is added to the data, therefore, is the product of the proportion of the image containing light matrix grains, 3.7%, and the fraction of the pixels that indicate motion.

The amount of motion in the sample when the first increment of flow is applied is plotted in Figure 6.3.2. Initially, there is a sharp peak, and the amount of motion decreases whilst the hydraulic head is increased further. At the peak value, the amount of accumulation exceeds the amount of erosion. This indicates that the area occupied by fine particles has increased relative to the previous image. The first two images are acquired when the flow rate is low, $\mathcal{O}\left(0.05 - 0.1\,cms^{-1}\right)$, and the fine fraction is present as a layer on the bottom of the pores. The increase in the flow rate appears to cause an expansion of the fine fraction; the particles take up more space in the FOV. Vardoulakis [2004] attributes this expansion to the mobilisation of the smaller grains of the fine fraction. The larger fine particles are not mobilised and block the pore throats preventing actual transport of fines. The mobile fines are confined to the pore they occupy and move around in this, instead of forming a layer at the bottom.

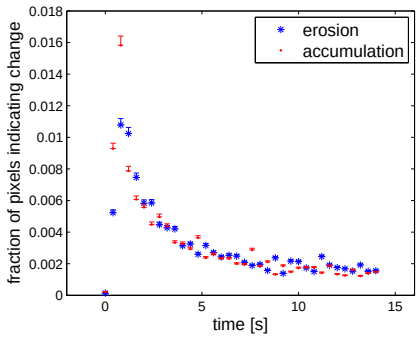

Test 1: Images are recorded at a frame rate of 2.5 fps. Motion is computed for an area of $80 \times 103\,mm$.

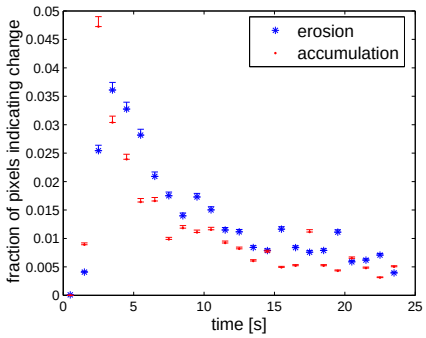

Test 7: Images are recorded at a frame rate of 1 fps. Motion is computed for an area of $100 \times 375\,mm$.

Figure 6.3.2: Amount of motion in the sample as a function of time. $^1/_3{}^{rd}$ of the maximum hydraulic head is applied in the first $10\,s$, followed by flow at constant head.

Another explanation is that fines enter the FOV from inside the sample. Given that there is little transport parallel to the flow direction, it is unlikely that a large amount of transport occurs in the direction perpendicular to the flow direction. The reported phenomenon is investigated further in Subsection 6.3.2, where the difference image from which these values are computed is inspected.

In tests 6 and 7, the time interval between images is greater than during test 1, resulting in more mobilisation per difference image. The difference between erosion and accumulation values is also greater in the images from those tests. Particles are transported further when the time interval is longer, thus more particles are transported beyond the FOV. As a result of this, the accumulation values that are measured are lower than when a short time interval is used. Manual inspection of the sample, as well as the total change measurements presented later in this Subsection, confirm that fines are transported out of the sample.

When the hydraulic head is initially applied, there is movement throughout the sample; this rapidly stops and movement continues only in distinct flow paths. In test 7, the FOV contains nearly the entire sample, including several flow paths. These are the cause of the fluctuations of the activity values that are observed. In test 1, the FOV contains only an area where the amount of motion drops relatively quickly.

To investigate the amount of motion at different depths in the sample, the FOV is divided into three equally large horizontal sections, and the activity in each of these is determined. Figure 6.3.3 reveals that there is more motion in the upper $^2/_3{}^{rd}$ of the sample. The initial increase in the area of the fine fraction is apparent in all three sections, however, this is much less in the lower part. Manual inspection, as well as analyses in the following two Subsections, indicates the formation of flow paths in the top $^2/_3{}^{rd}$ of the sample. The flow paths show a similar amount of activity for their entire length. This is reflected in the comparable activity patterns for the top and middle of the sample.

After the initial application of the hydraulic head, a constant head is applied to the sample for $10\,min$. Subsequently the hydraulic head is increased by a similar amount twice more, with a $10\,min$ constant head interval following each increase. The flow velocities in the sample corresponding to the three hydraulic heads are approximately $0.2\,cms^{-1}$, $0.4\,cms^{-1}$, and $0.7\,cms^{-1}$. The amount of motion for the entire test is shown in Figure 6.3.4. After the first application of hydraulic head, the further increments result in little additional motion. This suggests that the sample reaches an equilibrium state after the first application of flow, and this state is relatively insensitive to increases of the flow velocity.

The first increment of hydraulic head is relatively high and results in turbulent flow, $Re \sim 5$. This appears to be sufficient to mobilise most of the fine grains in the sample, as a result of which the amount of particle transport depends primarily on the free pore space. If the applied hydraulic head were lower, and the fluid drag force insufficient to mobilise all particles, increases of the hydraulic head would be expected result in the mobilisation of more particles.

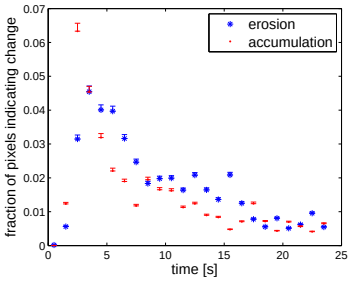

Test 7: top $1/3^{rd}$.

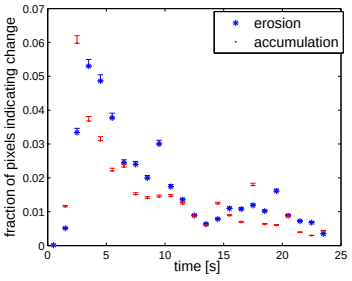

Test 7: middle $1/3^{rd}$.

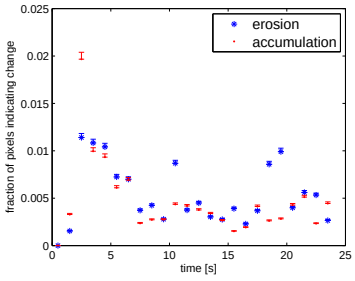

Test 7: bottom $1/3^{rd}$.

Figure 6.3.3: Amount of motion in the top, middle and bottom of the sample during the initiation of flow in test 7.

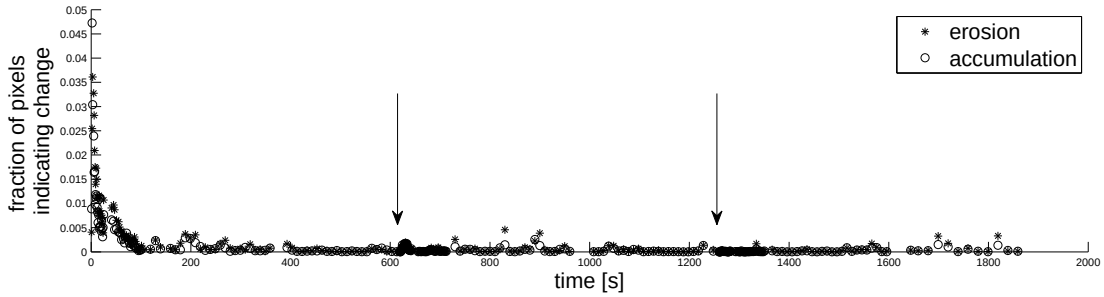

Figure 6.3.4: Motion in the sample throughout test 7. The flow rate is increased at $t = 0$, $t = 610\,s$ and $t = 1240\,s$.

During the constant head periods, several smaller peaks in activity correspond to the movement of clusters of fine grains. The erosion value exceeds the accumulation value; these groups of fines are either removed from the sample entirely, or they move perpendicular to the flow direction whereby they are obscured from the FOV. The increase of the amount of fines deposited on top of the sample indicates that fine grains are removed from the soil sample.

The total change difference images, used to study the evolution of the sample during suffusion, result from subtracting an image at time t_n from the first image. These images are used to construct a mass balance for the amount of fine grains in a section of the FOV. In Figure 6.3.5, the total amount of erosion and accumulation during test 7, after $600\,s$ and after $1850\,s$, is quantified. The difference between accumulation and erosion is indicative of the removal of fine grains. This difference is greater when the sample alone is considered than when the values are computed for the total FOV. In test 7, the total FOV includes the top load. During suffusion fine particles are removed from the sample and deposited in the top load; including this accumulation should lead to a closed mass balance.

The remaining imbalance is attributed to the difference between the porosity of the top load and the porosity of the sample. The sample has a lower porosity, thus the volume of sample required to contain a given mass of fines is greater than the volume of top load required to contain the same amount. As a result of this, the image area occupied by a mass of fines greater when this mass is present in the sample than when it is present in the top load.

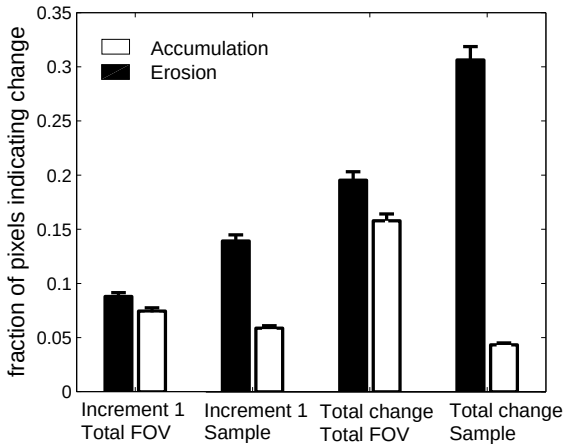

Figure 6.3.5: Accumulation and erosion in the sample and the entire FOV (including the sample and the top load). Increment 1 refers to the first 600 s after applying the flow. Total change refers to the entire duration of test 7.

At the end of test 7, a large amount of fines has been removed from the soil, and the sample appears to have reached an approximately stable condition. Test 8 is a continuation of test 7, whereby the sample is subjected to cycles of stopping and restarting the hydraulic head. The objective is to assess whether this leads to further suffusion. Table 6.3.1 lists the rates at which the hydraulic head is stopped and re-applied. The results of cycles 2 and 3 are shown in Figure 6.3.6.

Table 6.3.1: Stopping and restarting the flow.

Cycle number	Length of time in which flow is stopped [s]	Duration of no flow interval [s]	Length of time in which flow is re-applied [s]	Duration of constant flow interval [s]
1	10	10	10	20
2	10	10	20	20
3	2	10	2	20
4	2	10	2	20

All cycles show a peak in amount of motion during both the stopping and the restarting of fluid flow. This is similar to the motion that is observed when initially applying the hydraulic head to the sample. It can be attributed to the fine grains moving about within the pores that they occupy, not to a significant transport of material. The values of the peaks are higher for more rapid changes in the hydraulic head. A more rapid change in flow velocity exerts a greater force, mobilising more particles. When the hydraulic head is constant, the activity is reduced to a similar value for all cycles.

The effect of applying several cycles of stopping and restarting the flow on the mass balance of fines in the sample is shown in Figure 6.3.7. This shows that cycling the hydraulic head can lead to further erosion from the sample. In test 8, there is more accumulation than in test 7; this accumulation is indicative of re-arrangement of the fine fraction inside the sample. Mobilised fine particles get filtered within the soil, resulting in a higher accumulation values and a change in the structure of the sample. This process can only be inferred from possible permeability changes in outflow experiments, whereas it is directly observable using visualisation. The spatial distribution of the erosion and accumulation during suffusion is studied by regarding the difference images directly in the following Subsection.

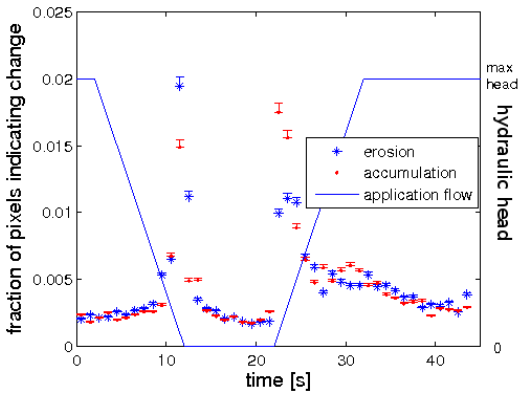

Cycle 2: Stopping and restarting flow by closing the valve in 10 s and opening in 10 s.

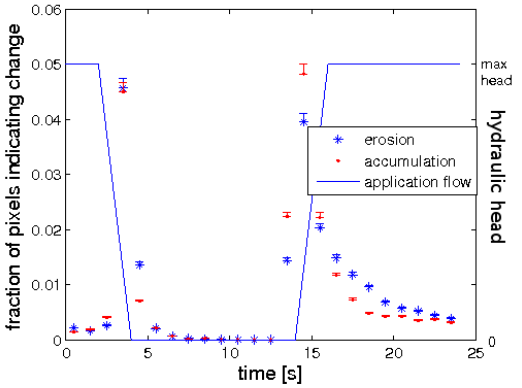

Cycle 3: Stopping and restarting flow by closing the valve in 2 s and opening in 2 s

Figure 6.3.6: Effect of stopping an restarting the flow on the amount of motion in the sample.

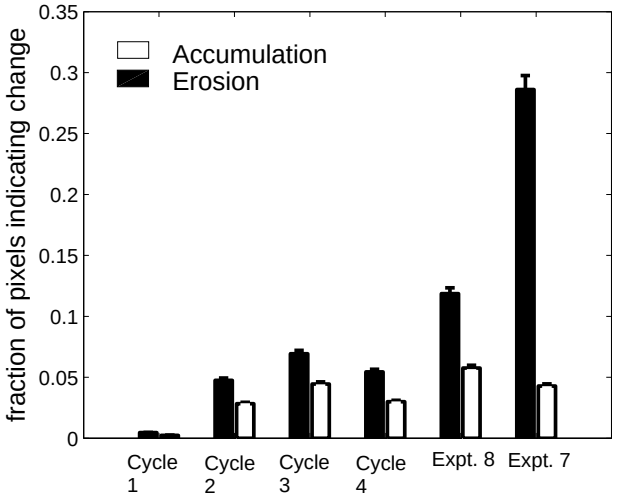

Figure 6.3.7: At the end of test 7, the sample is stable whilst the hydraulic head is at a maximum. This sample is used in test 8, where the flow is stopped and restarted 4 times, cycles $1-4$. This results in further erosion of fines from the sample.

6.3.2 Localisation of Motion

The activity values in the previous Subsection are indicative of changes occurring in the sample. Further understanding of what happens during suffusion can be obtained by studying the difference images directly in this Subsection.

When the flow is applied, a peak in the amount of accumulation is noted in Subsection 6.3.1. Vardoulakis [2004] attributes this to mobilisation of fine particles that are not transported beyond the pore that they occupy, an expansion of the fine fraction. Figure 6.3.8 shows the difference image that results in the high accumulation value. The locations that indicate the largest amount of accumulation appear to be in pores that contain free space; supporting the fine fraction expansion hypothesis.

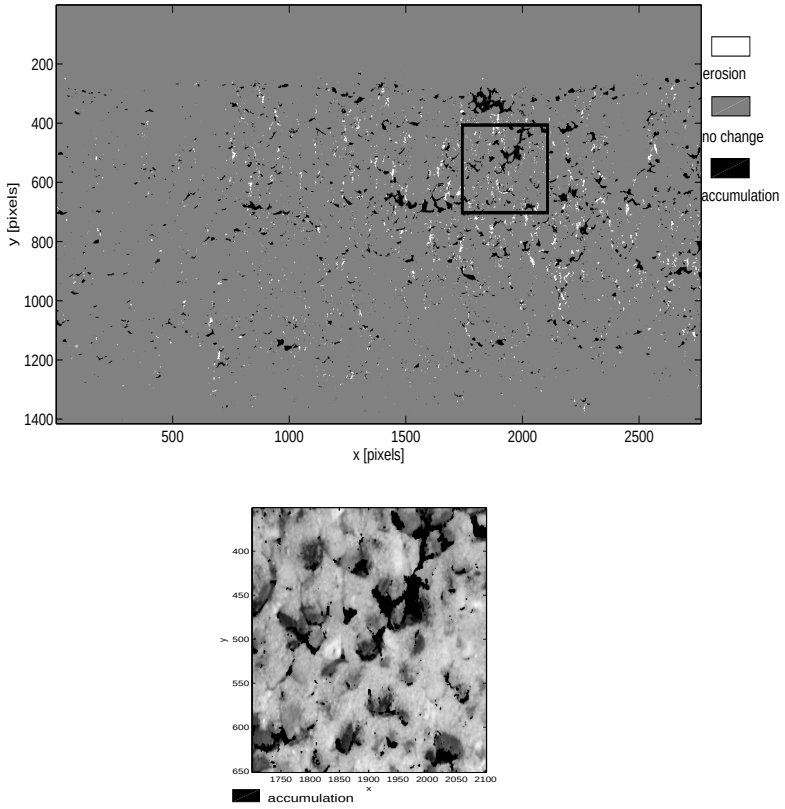

Figure 6.3.8: Difference image indicating a greater amount of accumulation than erosion. ($Scale: 111\,pixels = 10\,mm$)

During the remainder of the first application of the hydraulic head, the erosion values generally exceed the accumulation values. Figure 6.3.9 contains the total change difference image for the first $10\,s$ of flow. This is obtained by subtracting the 11^{th} image from the 1^{st} image. This clearly shows an accumulation of fine material on top of the sample; recall from Figure 6.3.1 that the sample is present between y coordinates 220 and 1380.

Manual inspection indicates that transport is concentrated in preferential flow paths that are located in the top $^2/_3{}^{rd}$ of the sample, and that erosion of fines predominantly occurs in the vicinity of these. To quantify the amount of movement occurring at different locations in the sample, a summation is made of the series of difference images that indicate motion. This sequence of motion difference images is obtained by subtracting each image from the previous one, and assigning a value of 1 to all pixels that indicate a change, either erosion or accumulation. The summation of the 25 motion difference images, spanning the first $25\,s$ of test 7, results in Figure 6.3.10. Areas that show motion multiple times are referred to henceforth as areas with a high activity. A high activity can be due to fines vibrating in place or to a sequence of fines moving past a location.

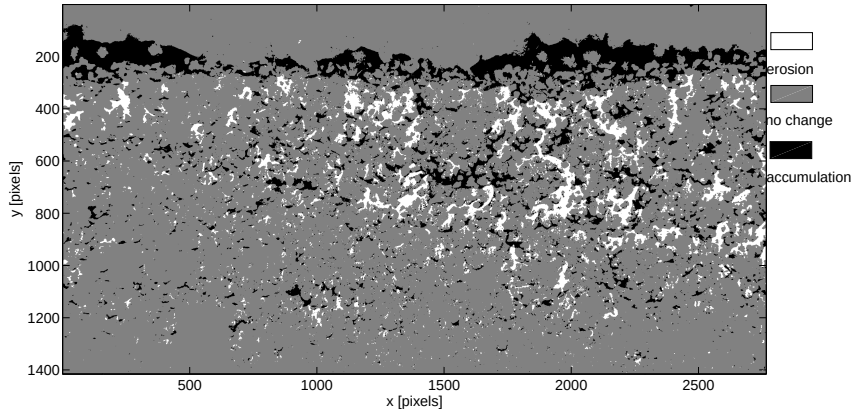

Figure 6.3.9: Sample change after the $10\,s$ application of the hydraulic head during test 7. $(Scale:\ 111\,pixels = 10\,mm)$

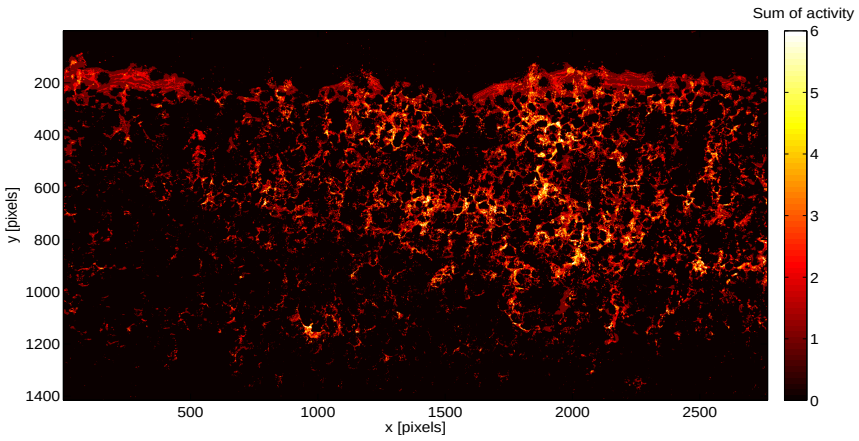

Figure 6.3.10: The summation of activity values for test 7 indicates that specific areas show movement multiple times, high activity, during the application of the hydraulic head. In the high activity areas, material is eroding and accumulating multiple times, indicating that fine particles are passing by. $(Scale:\ 111\,pixels = 10\,mm)$

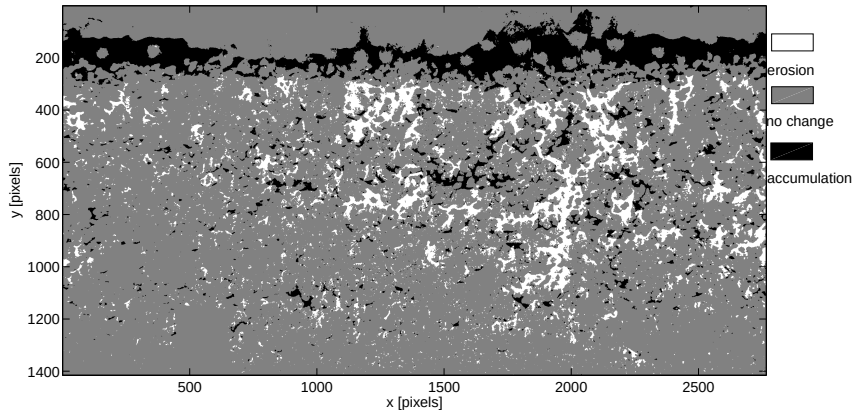

Figure 6.3.11: Total change in the appearance of the sample during the first $25\,s$ of test 7. $(Scale:\ 111\,pixels = 10\,mm)$

The total change during the first $25\,s$ of test 7 is obtained by subtracting the 25^{th} image from the 1^{st} image. The resulting total change difference image is shown in Figure 6.3.11. Erosion is concentrated predominantly in the regions that display a high activity in Figure 6.3.10. This strongly suggests that the eroded material is transported through the high activity areas, and not vibrating in place. The sample appears to develop preferential flow paths that transport the fine particles; these result in more erosion near these paths than in the rest of the sample.

The same areas show a high activity for the duration of test 7, as shown in Figure 6.3.12. Recall from Table 3.5.1 that during test 7 the hydraulic head is increased in 3 steps with 10 minutes of constant head between the increments. This suggests that a monotonic increase of the hydraulic head does not alter the spatial flow pattern significantly. The concentration of particle transport in specific regions of the sample suggest that the flow is channelled through these areas. More particles are eroded there, which is likely to result in an increased permeability of these flow paths. When the hydraulic head is increased, this is likely to result in a greater increase in the flow velocity in the more permeable areas than in the rest of the sample; thus the movement remains concentrated in these areas.

The formation and persistence of the preferential flow paths is indicative of a positive feedback whereby suffusion progressively increases the heterogeneity of the sample. Erosion leaves the soil more porous, causing a reduction in the filtration effect. Additionally, the flow rate is higher due to a higher permeability, thus more fine grains can be mobilised than in the rest of the sample where the flow rate is lower. This can lead to the depletion of fines in specific areas. The effect of this can also be seen when referring back to Figure 6.3.1.

At the walls, the porosity is higher than within the sample. This suggests that preferential flow paths will tend to initiate there. However, the development of preferential flow paths reported is related to heterogeneities within the plane of view, and not to a difference between the state of the sample at the wall and in the interior. This heterogeneity results from the placement of the sample. The objective was to pack a uniform sample, however, minor variations appear to be sufficient to initiate preferential flow paths.

The areas showing a high activity do not form connected paths, even when the assumption is made that areas with insufficient contrast also exhibit high activity, as shown in Appendix D.1. Flow paths have a component in the third dimension; this is due to contact between matrix grains and the sample walls. The reverse side of the sample displays a similar distribution of eroded and intact areas, but at different locations than in the FOV. The extent of the preferential flow paths in the third dimension appears to be less than the extent parallel to the FOV. This can be attributed to a higher porosity at the interface between the sample and the walls, which results in a higher flow rate there than in the interior of the sample.

During the cycles of flow in test 8, high activity occurs in different areas than in test 7, as shown in Figure 6.3.13. Stopping the flow leads to a settling of the fines due to gravity; this can remove particles that are filtered by straining or bridging. When the flow is restarted, fine grains are removed from the soil, as shown in Figure 6.3.14. During test 8, there is more activity and more erosion in the upstream section (the lower part) of the sample than during test 7.

An increase in the downstream porosity and permeability leads to an increase in the hydraulic gradient over the upstream section, which can result in more particle erosion. A high downstream porosity also reduces the probability of particle filtration, allowing more removal of material from the upstream section. As these experiments are conducted at high flow rates, the latter process is likely to dominate. In combination with the removal of filtered particles when the flow is stopped, this accounts for the additional removal of material from the sample during test 8. Furthermore, it demonstrates that the load history is important to include in a study of suffusion. This is examined further by visualising the evolution of motion with depth in the next Subsection.

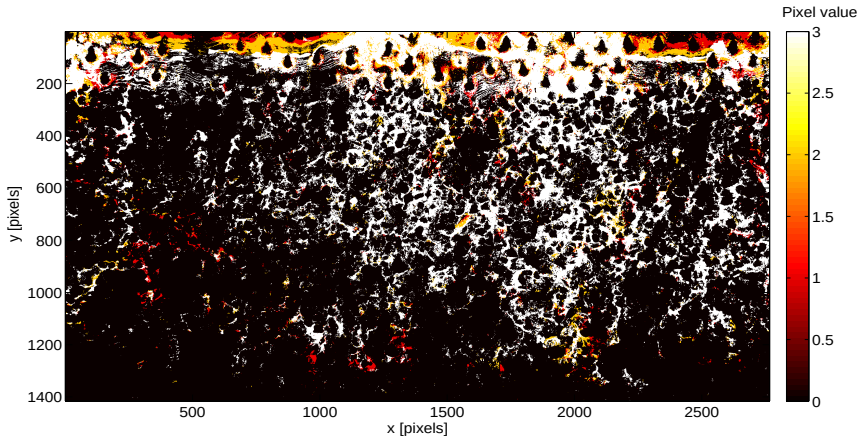

Figure 6.3.12: During test 7 three flow increments are applied, resulting in high activity in specific areas. The number of times that an area displays a high activity is indicated by the pixel value. Most areas that show high activity during one flow increment continue to do so for the other two increments. ($Scale: 111\,pixels = 10\,mm$)

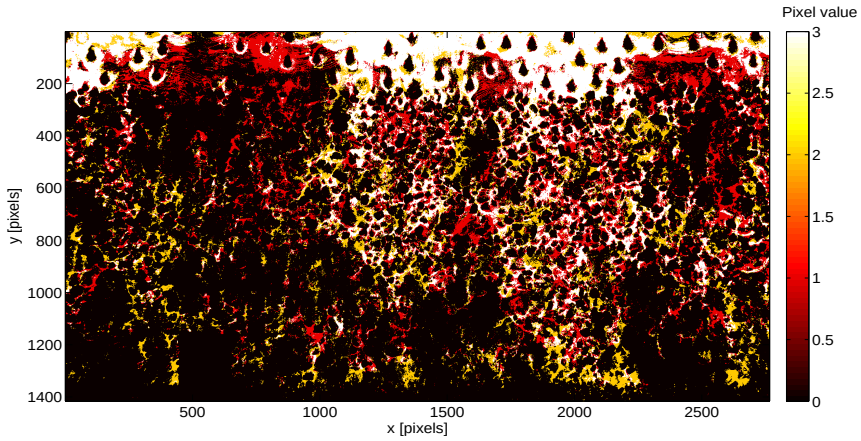

Figure 6.3.13: The locations of high activity during test 7 have a value of 1, and those for test 8 have a value 2; locations that show high activity in both tests have a value 3. ($Scale: 111\,pixels = 10\,mm$)

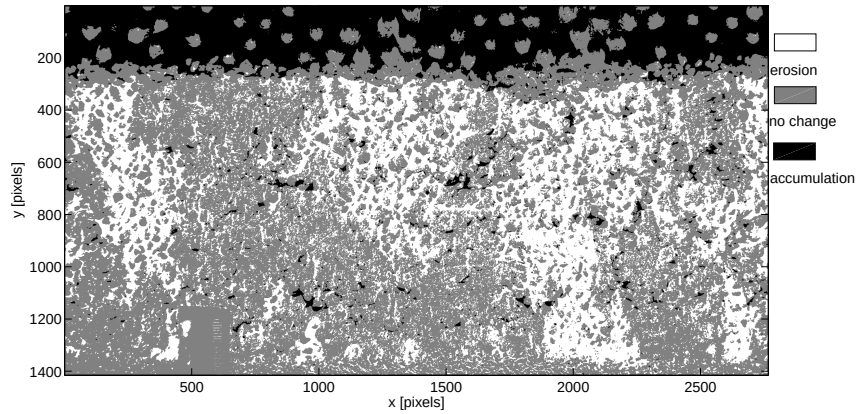

Figure 6.3.14: Total change in the appearance of the sample during tests 7 and 8. ($Scale: 111\,pixels = 10\,mm$)

6.3.3 Evolution of the Sample

The previous Subsection indicates that the location at which fines are mobilised is dependent on the current state of the sample and thereby on the load history. Temporal difference images are used to visualise this. These are constructed from difference images that show motion. A strip with the length of the sample and a width of 30 pixels ($\simeq D_{50coarse}$) is considered. The number of pixels showing motion is summed up over the width of the strip; resulting in a 1D vector whose entries are a measure of the amount of motion for the length of the sample. This is done for the complete sequence of difference images in tests 7 and 8. The resulting vectors are horizontally concatenated; resulting in a matrix where time progresses along the columns.

Figure 6.3.15 indicates the locations of the strips in the image that shows the state of the sample after test 7. Locations 1 and 2, for which the temporal difference images are shown in Figure 6.3.16, show a significant loss of fines. Little material is eroded at locations 3 and 4, for which the temporal difference images are shown in Figure 6.3.17. These images are used to quantify the amount of motion at different depths of the sample over time, which can be used to investigate some of the erosion and filtration processes that are described in literature Chapter 2.

Recall that the image acquisition rate during test 7 is not constant. To obtain a sufficient temporal resolution in periods when there is a large amount of activity, the acquisition rate is higher when the flow is applied or increased ($1\,fps$ for first 25 images, followed by $0.4\,fps$ for the subsequent 25 images, and $0.1\,fps$ for the remaining 50 images). After 10 minutes the hydraulic head is increased and the acquisition cycle is repeated. Test 8 starts at image 300, during this test the acquisition rate is constant at $1\,fps$.

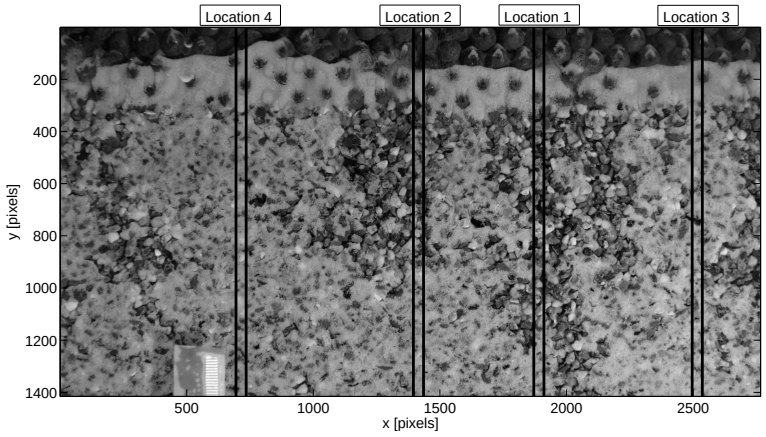

Figure 6.3.15: Locations of the sections used to construct the temporal difference images. ($Scale:\ 111\,pixels = 10\,mm$)

The instant the flow is started, most motion occurs in the upper $^2/_3{}^{rd}$ of the sample at locations 1 and 2. Within seconds, the activity in the top load indicates that fines are removed from the sample. The activity spreads to the lower part of the sample during the following $20\,s$.

At location 3, in the first cycle of 100 images, areas are distinguished where fine grains appear to vibrate in one location without being transported. This motion occurs over a short vertical distance for extended periods of time. Motion occurs around the bottom $^2/_3{}^{rd}$ in the first 40 images at location 4. Manual inspection indicates this is due to a flow path, with a diameter in the order of 60 pixels ($\simeq 2 \times D_{50coarse}$), that cuts across the strip. The path gets filled with fines, after which there is little further movement in this strip.

Increases of the hydraulic head are applied during images $100 - 110$ and $200 - 210$; these induce little additional movement at all locations. During flow at constant hydraulic head, there are distinct events of motion for a short time and over a significant vertical distance at locations 1 and 2. Manual inspection shows these events indicate transport, not vibration of particles.

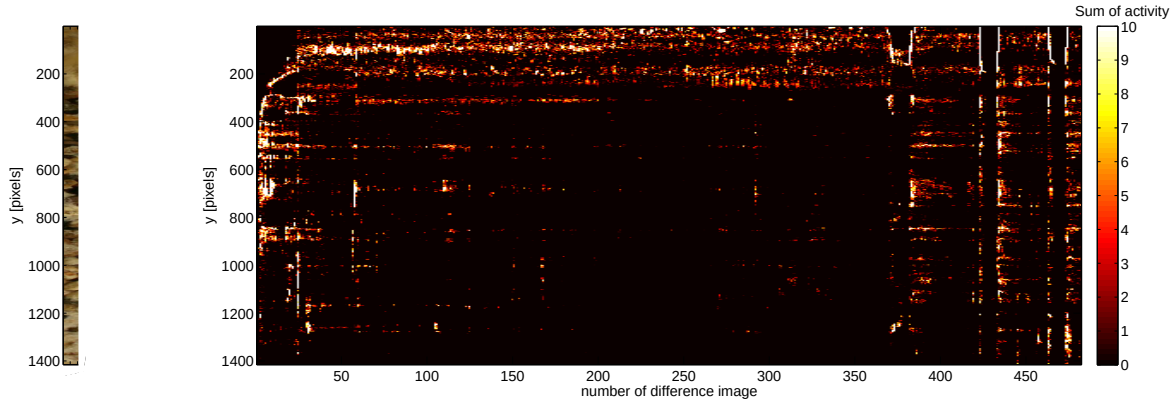

Location 1: Motion in sample around x coordinate 1890. ($Vertical\,scale : 111\,pixels = 10\,mm$)

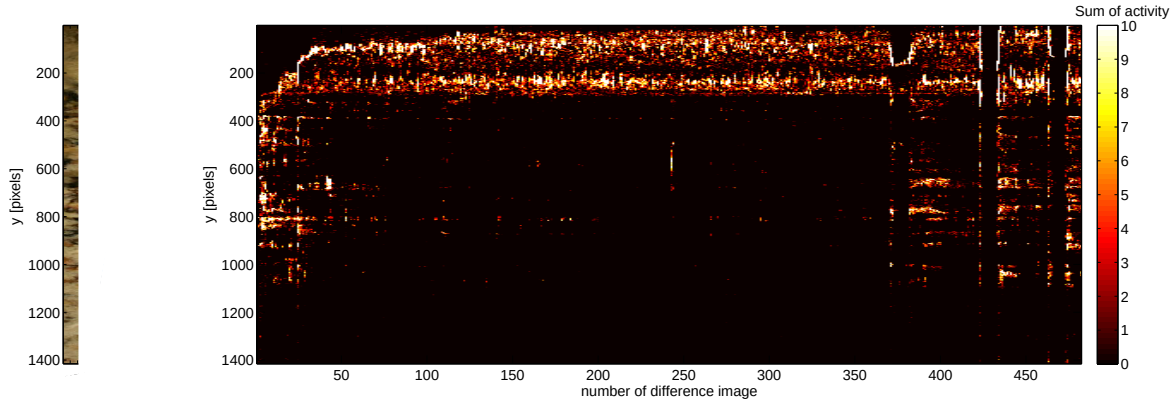

Location 2: Motion in sample around x coordinate 1415. ($Vertical\,scale : 111\,pixels = 10\,mm$)

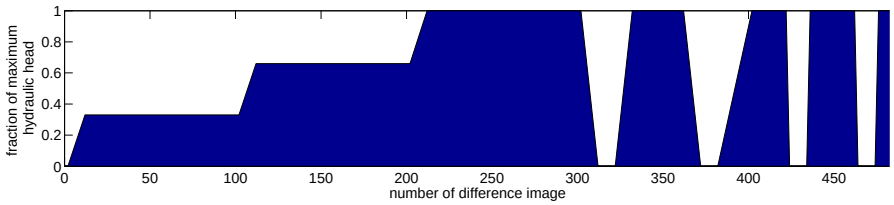

Fraction of the maximum hydraulic head applied.

Figure 6.3.16: Temporal difference images for locations where a large amount of erosion occurs.

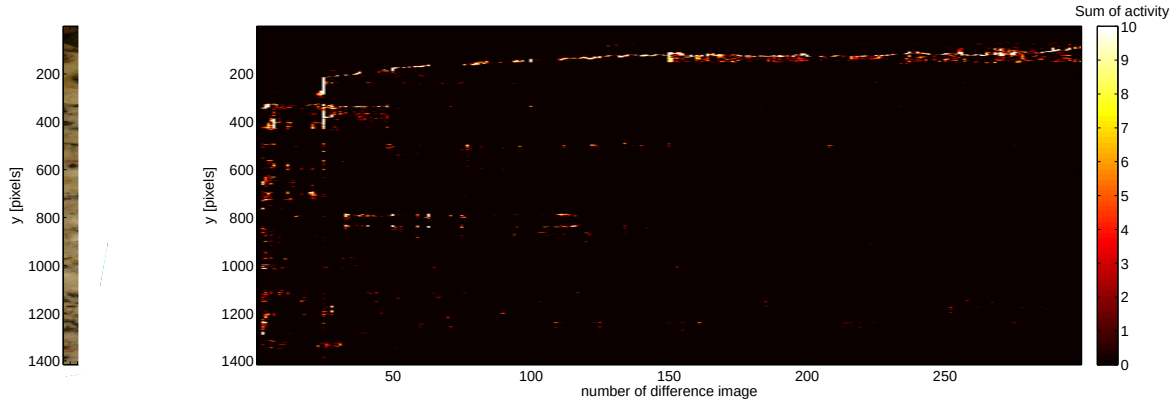

Location 3: Motion in sample around x coordinate 700. ($Vertical\,scale: 111\,pixels = 10\,mm$)

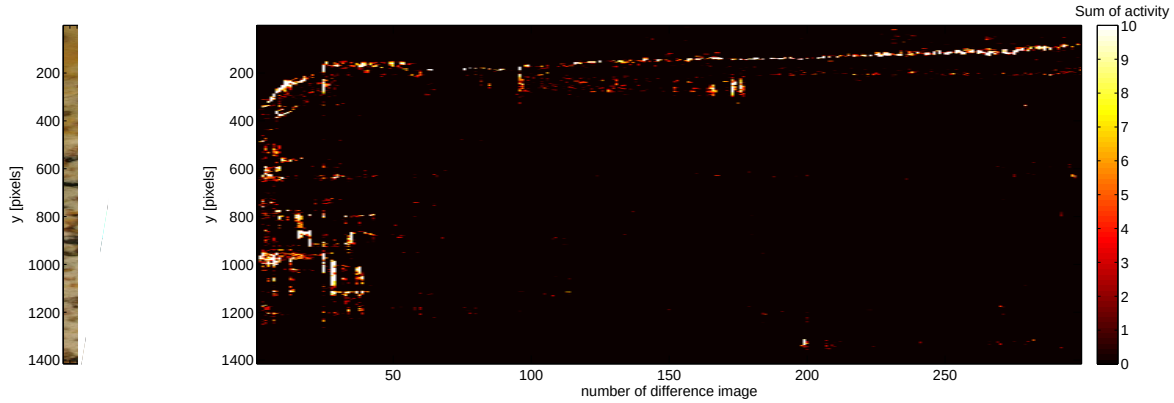

Location 4: Motion in sample around x coordinate 2500. ($Vertical\,scale: 111\,pixels = 10\,mm$)

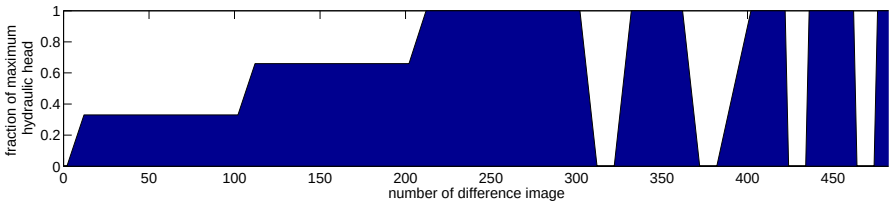

Fraction of the maximum hydraulic head applied.

Figure 6.3.17: Temporal difference images for locations where little erosion occurs.

In Appendix D.2, the total change in the appearance of the sample for each increment of the hydraulic head and each ensuing constant head interval is shown. This indicates that there is a significant amount of particle erosion during periods of constant hydraulic head.

The effect of the first cycle of stopping and restarting the flow in test 8 appears negligible; the subsequent cycles have more effect in locations 1 and 2. Stopping the flow results in instantaneous motion over the entire length of the sample; the fine particles settle. Restarting initiates motion for a longer period of time. This indicates that particles are not only mobilised but also transported. Settling can remove particles that initially blocked the pore constrictions by brigding. Restarting the flow can then lead to the removal of fines from those pores that were previously clogged. This leads to prolonged activity when the flow rate is restarted, as seen in these images.

At locations 3 and 4, no material is removed in test 7, and there is no activity during test 8. This supports the hypothesis that the downstream porosity has an important effect on particle transport occurring upstream. With less free pore space, the probability of filtration is higher, and fewer particles are transported. Additionally, the preferential flow paths channel the flow through more porous areas. This is likely to result in significantly lower flow velocities in the remainder of the sample. A lower fluid drag force is likely to result in less particle erosion.

The method of data analysis demonstrated in this Subsection complements those used in the previous two Subsections. This Section presents an initial application of different methods to interpret data from IS. Based on this, some conclusions are suggested, regarding both the process of suffusion and the method of data analysis, in the following Section.

6.4 Discussion and Evaluation

Quantitative image analysis using IS is found to be a useful tool to study suffusion. In this work, several methods of analysing the difference images resulting from IS are developed. These yield results that can be related to current hypotheses regarding the mechanisms of suffusion, erosion, and filtration, that are treated in Chapter 2. The different methods of data interpretation are evaluated in Subsection 6.4.1, and the phenomena that have been investigated in this work are discussed in Subsection 6.4.2.

6.4.1 On the Application of IS

IS is based on the assumption that movement of the fine fraction exposes the underlying coarse matrix. As these two materials have a different intensity, the locations where material erodes and accumulates stand out. The method is suited to the experimental setup used in this work; it is used to quantify of the amount of mobile material and not the displacement distance, therefore, it is less sensitive to out of plane motion and longer time intervals between successive images. Two approaches are used; one where the amount of instantaneous motion is quantified, and one where the difference with respect to an earlier situation is determined. The corresponding measures, the amount of motion and the total change in sample appearance, are ratios of the area indicating a movement to the total area that is examined, and do not correspond directly to physical quantities.

The total change in the sample appearance is an indicator for the removal of fine grains from the sample. When the accumulation of fine grains in the top load is accounted for, the measured amount of erosion and accumulation differ by a small amount. This indicates that net transport perpendicular to the plane of view has a limited effect on the mass balance obtained using IS. If the mass of particles that is removed from the sample were independently determined, this could be used to calibrate the amount of erosion that is measured in the images.

The measure of the amount of motion in itself is not enough to determine whether fine grains are being transported. High motion values are induced by fluctuations of the flow rate; stopping the flow causes motion that is associated with fine grains settling within the pore they occupy, not with transportation through the sample. Furthermore, the vibrating grains can result in a high amount of motion, as also noted by Skempton and Brogan [1994]. To quantify transport, the motion data must be interpreted in combination with data based on the total change in appearance of the sample or manual inspection.

IS can be used to establish whether an equilibrium is reached more accurately than outflow experiments. The difference between internal rearrangement of the fine fraction, due to an equal amount of erosion and filtration, and no movement of the fine grains, is directly observed using visualisation. In outflow experiments this has to be inferred from possible changes in permeability.

The measured motion could underestimate the amount of movement of the fines; this happens when they erode and accumulate at the same location during the interval between successive images. This can occur when the concentration of suspended fine particles is high, e.g. in preferential flow paths. In the current tests, manual inspection indicates no cases where this occurred, but this is not conclusive evidence. When a non uniform fine fraction is used, the probability of identical fine particles eroding and accumulating on the same place is much reduced.

The methods of IS used here are significantly improved by a clear distinction between the fine and the coarse fractions. In combination with a more constant source of illumination, this reduces the uncertainty value. In that case, the proportion of the image area that contains fine particles can be determined. The areal concentration of fines can be used to scale the amount of motion observed; as opposed to the total image area that is currently used. This allows the study of the effect of the concentration of fines on the process of suffusion.

The images analysed in this Chapter have a FOV of $253 \times 169\,mm$. To study the effect of the structure of the sample on erosion and filtration on the pore scale, IS can be applied to images with a smaller FOV, $10 \times 14\,mm$. The same methods of image processing and data analysis can be applied to these images, as shown in Appendix D.3.

In this work, three methods are used to analyse the difference images. Firstly, the data is spatially averaged and studied over time in scatter plots and bar graphs. This can be used to relate the applied hydraulic boundary conditions to the amount of particle movement in the sample. Secondly, the 2D spatial context of the difference images is analysed. Summations of sequences of motion difference images indicate locations where material is transported for extended periods of time. Difference images that span a longer time interval indicate the changes in the sample structure as a result of particle transport. Thirdly, the effect of the load history on the transport of particles is studied. The amount of motion in a 1D vertical slice of the sample is plotted over time, with sample height along the $y - axis$ and time progressing along the $x - axis$, resulting in what is referred to here as a temporal difference image. These images are used to analyse the coupling between the sample structure, which changes due to suffusion, and particle transport.

From the results of this initial investigation, it can be concluded that IS presents a tool to complement permeameter experiments for the study of suffusion. Further work includes the design of an experimental setup that allows for the calibration of visualisation data with effluent and permeability measurements.

6.4.2 On the Process of Suffusion

The number of experiments that is analysed in this Chapter is limited, and no general conclusions can be drawn from the reported observations. Tentative suggestions are made regarding the effect of suffusion on the soil sample; in a flow regime that tends to turbulence, with $5 < Re < 20$.

The highest motion values are observed when the flow is applied or stopped. When there is no flow, fines form a layer on the bottom of the pores in the coarse matrix. Application of flow causes particles to move about within the pores, whereby they occupy a larger area in the FOV, as illustrated in Figure 6.4.1. This suggests that fluid flows within the pores of both the fine and the coarse fractions. The expansion of the fine fraction is also noted by Skempton and Brogan [1994], who report an increase in the total sample permeability as a result of this. Both the expansion and the relation between the porosity of the fine fraction and the sample permeability are accounted for in a suffusion model presented by Vardoulakis [2004].

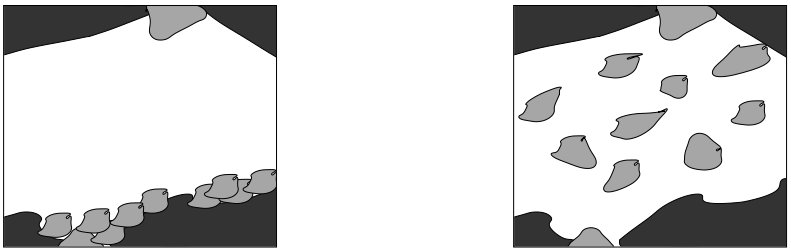

Figure 6.4.1: Expansion of the fine fraction. Without flow (left) the fine grains are present as a layer on the bottom of the pores in the coarse matrix. When the fines are mobilised, but not yet transported due to larger fines clogging the pore constrictions, the fine fraction occupies a greater area in the FOV (right).

In this work, disjoint events where collective groups of fines are eroded, lend further support to the consideration of fluid flow inside the fine fraction. If flow occurred only at the surface of the fine fraction, one would expect fines to be eroded from the interface of the fines and the fluid towards the interface of the fines and the coarse grains, as illustrated in Figure 6.4.2. The detachment of entire groups of particles suggests that fluid drag forces are acting over the entire volume of the fine fraction, as shown in Figure 6.4.3. Bed load particle entrainment also involves the erosion of collective groups of particles and this is modelled by incorporating fluid flow in the bed, by e.g., by Coleman and Nikora [2008].

Figure 6.4.2: No fluid flow within the fine fraction (light coloured) leads to erosion at the interface between the fluid (white) and the fine fraction.

Figure 6.4.3: Fluid flow both in the free pore space and in the pores of the fine fraction exerts drag forces on all particles and can lead to erosion of groups of fine particles.

Many authors report that suffusion does not remove all fine grains from the soil e.g., Skempton and Brogan [1994], Moffat and Fannin [2006], Bendahmane et al. [2008]. The current tests show that localised erosion occurs when the flow rate is monotonically increased; some areas become depleted of fines, and a steady state is reached whereby no particles are moving. Additionally, it is observed that movement of fine particles continues for a significantly longer period of time in the areas of the sample that become more eroded than in the rest of the soil. When the flow is stopped and restarted, this induces a significant amount of additional erosion and movement in regions where little motion occurred during the first period of flow.

Initially, more fine particles are removed from the downstream than from the upstream portion of the sample. This suggests that filtration occurs; particles present near the outlet of the sample have a lower probability of being filtered by bridging or straining than the particles that are further upstream and travel a longer distance inside the sample. Filtered particles clog the pores, preventing further erosion from upstream sections.

Small variations in the sample structure and hydraulic conditions within the plane of view, in the horizontal direction, are observed to lead an amplification of the heterogeneity of the sample. Locally, a higher rate of erosion results in a greater porosity that reduces the probability of filtration. Possibly the flow velocity in these areas increases, as the fluid flow is channelled through the more permeable sections of the sample. This positive feedback is an explanation for the depletion of fines in specific areas, preferential flow paths, whereas the remainder of the sample retains most of the fines particles.

When the flow is stopped, the filtered particles settle, opening the clogged pores. When the flow is restarted, less filtration occurs; prior erosion in the downstream section of the sample has increased the porosity. Many areas where erosion takes place after restarting the flow are upstream of sections where a large amount of fines are eroded initially. This is a strong indication that the filtration of the fine fraction plays an important role, and should be included explicitly in suffusion models; even in this experiment where the $D_{50\,course}/D_{50\,fine} = 10$.

Preferential flow occurs due to structural heterogeneity in soils, and can play an important role in flow processes [Mooney and Morris, 2008]. Results from tests outlined in this work suggest that heterogeneities can be amplified during suffusion. Most suffusion studies reported in literature make no mention of preferential flow paths, e.g. Bendahmane et al. [2008], Marot et al. [2009], or only find them in some tests but not in others, e.g., Fannin and Moffat [2006]. Further work is required to assess under what experimental conditions preferential flow paths form, and whether these are present in field situations. Preferential flow in laboratory soil samples is studied using image analysis and dye tracers by e.g., Mooney and Morris [2008]. Methods to study of preferential flow in the interior of soil samples include resign impregnation and CT scans. For the application of these and other methods the reader is referred to a review by Allaire et al. [2009].

The method of IS presented in Chapter 6 cannot be used to study the deformation of the coarse matrix due to suffusion. Initially, the matrix grains are partially covered by fine particles, the removal of these alters the appearance of the sample to such an extent that comparing the initial and final images does not allow an unambiguous interpretation of the matrix movements. To study if there is mobilisation of the matrix, an experimental setup whereby the fine fraction and the fluid are fully transparent is required. PIV can be used to determine the velocity field of the matrix.

In the experiments performed in this work, the hydraulic head is increased in large steps. To investigate the effect of hydraulic gradient and flow velocity on suffusion, a refinement of the step size is required. This is, furthermore, important to study the effect of the rate of application of flow on the process. The experimental setup is improved when the hydraulic head and the flow rate can be measured during, and not only after, the experiments. These quantities, however, are averaged over the entire sample, and test results indicate the amplification of heterogeneity inside the sample. The fluid velocity within preferential flow paths can be studied by means of visualisation of a front of tracer dye.

The use of visualisation and image analysis for the study of suffusion are explored in this work. This allows the study of erosion and filtration processes that can be relevant in conceptual models for suffusion. The results indicate that the load history plays an important role in determining both the amount of material that is eroded from the sample, and the locations where erosion occurs. This suggests that the proportion of fines that is removed from the sample is underestimated when it is based on experiments where the flow rate is monotonically increased. Further experimental work is required to establish whether the initial observations are representative for the mechanism of suffusion in general. Suggestions are made to improve the experimental setup both to improve the quality of the images for analysis and to improve the control of the boundary conditions.

Chapter 7

Conclusions

The objective of this work is to investigate the use of quantitative visualisation for the study of suffusion. Most current experimental research in this field makes use of outflow experiments, where the mass of eroded material and the hydraulic conditions are measured. The conceptual models that are based on these experiments contain assumptions and constitutive relations that are related to specific experimental conditions. Visualisation enables the direct observation of the sample during suffusion, which can lead to an improved understanding of the processes that occur. A physical description of these processes can replace empirical expressions and result in more generally valid models. Different methods of image analysis are considered for the study of suffusion.

Particle image velocimetry (PIV) proves to be unsuccessful to determine the velocity field of the mobilised fine particles using this experimental setup. A prerequisite for PIV is that the field of view (FOV) can be divided into interrogation windows that retain their appearance as they are transported. These windows are identified in successive images, on the basis of which a velocity field is constructed. During suffusion, the displacement field is discontinuous; only the fine grains are transported, whereas the coarse grains remain stationary. The appearance of the windows containing both fine and coarse grains changes, and no accurate velocity field can be computed. Reducing the size of the windows to that of a fine particle results in ambiguity as the windows contain too little information to accurately identify them in successive images. A significant increase in the image acquisition rate, to minimise the change in the appearance of the interrogation windows, in combination with algorithms allowing for deformation of the windows is a possible improvement, but this is beyond the scope of this study.

Particle tracking (PT) is a Lagrangian analysis technique, whereby the paths of individual tracer particles are reconstructed. The main limitation of PT applied in the current setup, is a loss of tracer particles as they are obscured behind other particles. This can be resolved by use of both a transparent fluid and a fully transparent porous medium, so that only tracer particles stand out. Multiple cameras can be used to perform 3D PT using stereophotogrammetry, as is done for experimental fluid mechanics [Ouellette et al., 2006]. A further limitation in this work is the relatively low image acquisition rate; this results in large particle displacements between images. To accurately determine tracks, the spacing between tracer particles must be significantly less than the displacement distance.

With the setup used, image subtraction yields the most robust data. This Eulerian measurement method is based on quantifying the change in the appearance of the sample, as opposed to identifying the same particle or section of the FOV in successive images. The main benefit is that the method is invariant to out of plane movements; the main drawback is that the data is ambiguous. A change in the sample appearance can be due to particle movement in any direction and over any distance. To overcome this, several novel methods of data interpretation are developed and applied to images from suffusion experiments. There are strong indications that suffusion can lead to localised phenomena, and that the coupling between soil structure and particle transport leads to hysteresis effects. Based on the limited data set, however, no definitive conclusions can drawn.

Visualisation provides a valuable tool to complement existing outflow experiments. To model suffusion, an Eulerian description of how the soil structure, and therefore the flow regime, changes, and a Lagrangian measure of the behaviour of individual particles are complementary. Image subtraction, using the techniques of data interpretation developed in this work, can be applied to provide the former, 3D PT is a good method to investigate the latter. In this manner, the use of concepts from the fields of filtration, erosion, and granular flow for the description of the process of suffusion can be investigated. An accurate physical description of suffusion is important to extrapolate laboratory results to field situations and make a reliable assessment of the consequences of suffusion.

Bibliography

B. Aberg. Void ratio of noncohesive soils and similar materials. *Journal of Geotechnical Engineering*, 118 (9):1315–1334, 1992.

B. Aberg. Washout of grains from filtered sand and gravel materials. *Journal of Geotechnical Engineering*, 119(1):36–53, 1993.

S. E. Allaire, S. Roulier, and A. J. Cessna. Quantifying preferential flow in soils: A review of different techniques. *Journal of Hydrology*, 378(1-2):179–204, 2009.

C. Ancey and P. Evesque. Frictional-collisional regime for granular suspension flows down an inclined channel. *Phys. Rev. E*, 62(6):8349–8360, 2000.

T. Baumann and C.J. Werth. Visualization and modeling of polystyrol colloid transport in a silicon micromodel. *Vadose Zone Journal*, 3(2):434–443, 2004.

F. Bendahmane, D. Marot, and A. Alexis. Experimental parametric study of suffusion and backward erosion. *Journal of Geotechnical and Geoenvironmental Engineering*, 134(1):57–67, 2008.

D. Blair and E. Dufresne. The matlab particle tracking code repository. http://physics.georgetown.edu/matlab/, June 2010.

S. Bonelli and D. Marot. On the modelling of internal soil erosion. *International Association for Computer Methods and Advances in Geomechanics*, 2008.

A. Bouddour, J. L. Auriault, and M. Mhamdi-Alaoui. Erosion and deposition of solid particles in porous media: Homogenization analysis of a formation damage. *Transport In Porous Media*, 25(2):121–146, 1996.

L. Bucciantini, A. Farina, and A. Fasano. Flows in porous media with erosion of the solid matrix. *Networks and Heterogeneous Media*, 5(1):63–95, 2010.

S. E. Coleman and V. I. Nikora. A unifying framework for particle entrainment. *Water Resources Research*, 44(4):W04415, 2008.

E. A. Cowen and S. G. Monismith. A hybrid digital particle tracking velocimetry technique. *Experiments In Fluids*, 22(3):199–211, 1997.

J.C Crocker and D.G. Grier. Methods of digital video microscopy for colloidal studies. *Journal of Colloid and Interface Science*, 179:298–310, 1996.

A.H de Zwart. *Investigation of Clogging Processes in Unconsolidated Aquifers near water supply wells*. PhD thesis, Delft University of Technology, 2007.

A. Drescher and G. de Josselin de Jong. Photoelastic verification of a mechanical model for the flow of a granular material. *Journal of the Mechanics and Physics of Solids*, 20(5):337 – 340, 1972.

R. J. Fannin and R. Moffat. Observations on internal stability of cohesionless soils. *Geotechnique*, 56(7): 497–500, 2006.

M. Foster, R. Fell, and M. Spannagle. The statistics of embankment dam failures and accidents. *Canadian Geotechnical Journal*, 37(5):1000–1024, 2000.

Y. X. Gao and M. L. Kilfoil. Accurate detection and complete tracking of large populations of features in three dimensions. *Optics Express*, 17(6):4685–4704, 2009.

L. Gui and W. Merzkirch. A comparative study of the mqd method and several correlation-based piv evaluation algorithms. *Experiments In Fluids*, 28(1):36–44, 2000.

L. C. Gui and W. Merzkirch. A method of tracking ensembles of particle images. *Experiments In Fluids*, 21(6):465–468, 1996.

B. Indraratna and S. Radampola. Analysis of critical hydraulic gradient for particle movement in filtration. *Journal of Geotechnical and Geoenvironmental Engineering*, 128(4):347–350, 2002.

B. Indraratna and F. Vafai. Analytical model for particle migration within base soil-filter system. *Journal of Geotechnical and Geoenvironmental Engineering*, 123(2):100–109, 1997.

S. Kakuturu and L. N. Reddi. Mechanistic model for self-healing of core cracks in earth dams. *Journal of Geotechnical and Geoenvironmental Engineering*, 132(7):890–901, 2006.

T. C. Kenney and D. Lau. Internal stability of granular filters. *Canadian Geotechnical Journal*, 22(2): 215–225, 1985.

A. Keshavarzy and J. E. Ball. An application of image processing in the study of sediment motion. *Journal of Hydraulic Research*, 37(4):559–576, 1999.

M. L. Kilfoil. Particle pretracking and tracking and 2d feature finding. http://www.physics.mcgill.ca/ kilfoil/downloads.html, July 2010.

V.D. Le, D. Marot, L. Thorel, J. Garnier, and P Audrain. Centrifuge modeling of an internal erosion mechanism. Number 210 in International Conference on Scour and Erosion, pages 629–638, 2010.

M. Locke, B. Indraratna, and G. Adikari. Time-dependent particle transport through granular filters. *Journal of Geotechnical and Geoenvironmental Engineering*, 127(6):521–529, 2001.

M. Maknoon and T. F. Mahdi. Experimental investigation into embankment external suffusion. *Natural Hazards*, 54(3):749–763, 2010.

N.A. Malik, T. Dracos, and D.A. Papantoniou. Particle tracking velocimetry in three-dimensional flows. *Experiments in Fluids*, 15:279–294, 1993.

D. Marot, F. Bendahmane, F. Rosquoet, and A. Alexis. Internal flow effects on isotropic confined sand-clay mixtures. *Soil & Sediment Contamination*, 18(3):294–306, 2009.

R. A. Moffat and R. J. Fannin. A large permeameter for study of internal stability in cohesionless soils. *Geotechnical Testing Journal*, 29(4):273–279, 2006.

S. J. Mooney and C. Morris. Morphological approach to understanding preferential flow using image analysis with dye tracers and x-ray computed tomography. *Catena*, 73(2):204–211, 2008.

N Mori and K Chang. Introduction to mpiv, 2003. http://www.oceanwave.jp/softwares/mpiv.

D. Muir Wood. The magic of sands. *Canadian Geotechnical Journal*, 44:1329–1350(22), 2007.

N. Ochiai, E. L. Kraft, and J.S. Selker. Methods for colloid transport visualization in pore networks. *Water Resources Research*, 42(12):W12S06, 2006.

N.T. Ouellette, H.T. Xu, and E. Bodenschatz. A quantitative study of three-dimensional lagrangian particle tracking algorithms. *Experiments In Fluids*, 40(2):301–313, 2006.

B. Pan, K.M. Qian, H.M. Xie, and A. Asundi. Two-dimensional digital image correlation for in-plane displacement and strain measurement: a review. *Measurement Science & Technology*, 20(6):062001, 2009.

E. Papamichos and I. Vardoulakis. Sand erosion with a porosity diffusion law. *Computers and Geotechnics*, 32(1):47–58, 2005.

A.N. Papanicolaou, P. Diplas, M. Balakrishnan, and C.L. Dancey. Computer vision technique for tracking bed load movement. *Journal of Computing In Civil Engineering*, 13(2):71–79, 1999.

J.F. Peters and E.S. Berney. Percolation threshold of sand-clay binary mixtures. *Journal of Geotechnical and Geoenvironmental Engineering*, 136(2):310–318, 2010.

L. Portela and R. Oliemans. Possibilities and limitations of computer simulations of industrial turbulent dispersed multiphase flows. *Flow, Turbulence and Combustion*, 77:381–403, 2006.

L. Preziosi and A. Farina. On darcy's law for growing porous media. *International Journal of Non-linear Mechanics*, 37(3):485–491, 2002.

A. Radice and F. Ballio. Double-average characteristics of sediment motion in one-dimensional bed load. *Acta Geophysica*, 56:654–668, 2008.

A. Radice, S. Malavasi, and F. Ballio. Solid transport measurements through image processing. *Experiments In Fluids*, 41(5):721–734, 2006.

L.N. Reddi and M.V.S. Bonala. Critical shear stress and its relationship with cohesion for sand-kaolinite mixtures. *Canadian Geotechnical Journal*, 34(1):26–33, 1997.

L.N. Reddi, I.M. Lee, and M.V.S. Bonala. Comparison of internal and surface erosion using flow pump tests on a sand-kaolinite mixture. *Geotechnical Testing Journal*, 23(1):116–122, 2000.

K.S. Richards and K.R. Reddy. Critical appraisal of piping phenomena in earth dams. *Bulletin of Engineering Geology and the Environment*, 66:381–402, 2007.

K.S. Richards and K.R. Reddy. True triaxial piping test apparatus for evaluation of piping potential in earth structures. *Geotechnical Testing Journal*, 33(1):83–95, 2010.

H.J. Roarty and M.S. Bruno. Laboratory measurements of bed load sediment transport dynamics. *Journal of Waterway Port Coastal and Ocean Engineering*, 132(3):199–211, 2006.

T.K. Sen and K.C. Khilar. Review on subsurface colloids and colloid-associated contaminant transport in saturated porous media. *Advances in Colloid and Interface Science*, 119(2-3):71 – 96, 2006.

A.A. Shapiro and P.G. Bedrikovetsky. A stochastic theory for deep bed filtration accounting for dispersion and size distributions. *Physica A: Statistical Mechanics and its Applications*, 389(13):2473 – 2494, 2010.

A.W. Skempton and J.M. Brogan. Experiments on piping in sandy gravels. *Geotechnique*, 44(3):449–460, 1994.

C. Slominski, M. Niedostatkiewicz, and J. Tejchman. Application of particle image velocimetry (piv) for deformation measurement during granular silo flow. *Powder Technology*, 173(1):1–18, 2007.

D Sterpi. Effects of the erosion and transport of fine particles due to seepage flow. *International Journal of Geomechanics*, 3(1):111–122, 2003.

F. Sugita and R.W. Gillham. Pore scale variation in retardation factor as a cause of nonideal reactive breakthrough curves: 3. column investigations. *Water Resources Research*, 31(1):121–128, 1995.

J.K. Sveen and E.A Cowen. Quantitative imaging techniques and their application to wavy flow. *World Scientific*, 2004.

K Terzaghi, R.B Peck, and G Mesri. Soil mechanics in engineering practice. pages 81–83, 1996.

S.S. Tomlinson and Y.P. Vaid. Seepage forces and confining pressure effects on piping erosion. *Canadian Geotechnical Journal*, 37(1):1–13, 2000.

B. Tremblay and K. Oldakowski. Modeling of wormhole growth in cold production. *Transport In Porous Media*, 53(2):197–214, 2003.

I. Vardoulakis. Fluidisation in artesian flow conditions: Hydromechanically unstable granular media. *Geotechnique*, 54(3):165–177, 2004.

I. Vardoulakis, M. Stavropoulou, and P. Papanastasiou. Hydro-mechanical aspects of the sand production problem. *Transport in Porous Media*, 22:225–244, 1996.

I. Vardoulakis, S Diebels, and H. Steeb. Modelling erosive processes in the framework of the theory of porous media. In *Tagungsband des Symposiums "Grenzschicht Wasser und Boden, Phaenomene und Ansaetze"*, 2005.

C.F. Wan and R. Fell. Assessing the potential of internal instability and suffusion in embankment dams and their foundations. *Journal of Geotechnical and Geoenvironmental Engineering*, 134(3):401–407, 2008.

J.S. Yoon, J.T. Germaine, and P.J. Culligan. Visualization of particle behavior within a porous medium: Mechanisms for particle filtration and retardation during downward transport. *Water Resources Research*, 42(6):W06417, 2006.

Appendix A

Particle Image Velocimetry

A.1 Uniform Displacement

To investigate whether the contrast in the sample is sufficient to perform PIV using the the MQD algorithm, a uniform displacement is imposed on a representative image. As the entire image is shifted, the spatial gradient of the displacement field is zero. Interrogation windows of 32×32 pixels are applied.

The calculated displacement field is shown in Figure A.1.1. The maximum error in the determined displacement is 0.47% of the applied displacement when the image is moved a distance of 1 pixel. Increasing the displacement of the image to 3 pixels reduces the error to 0.08%.

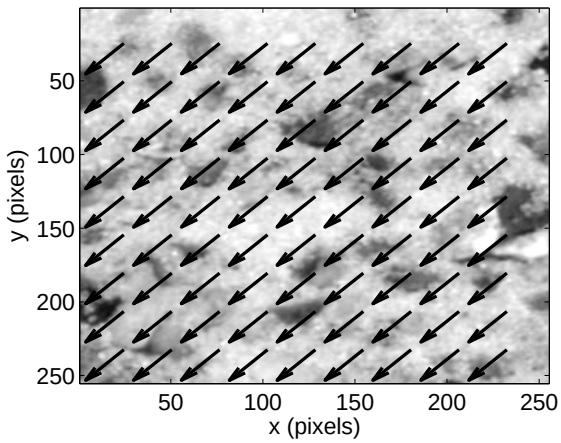

Figure A.1.1: The vectors determined using the MQD algorithm are shown on top of the image they are determined for. The displacement indicated by the vectors corresponds well with the movement that is imposed on the image. ($Scale: 111\,pixels = 10\,mm$)

A.2 Grayscale Stretching

The grayscale pixel intensities are stored as 8 bit integers. The fine fraction has an intensity in the range of 40 to 200. Values below 40 are assigned a value 0 and values above 200 are assigned a value 255. The values in between are linearly mapped on a scale from 1 to 255; resulting in a greater contrast in the fine fraction as shown in Figure A.2.1.

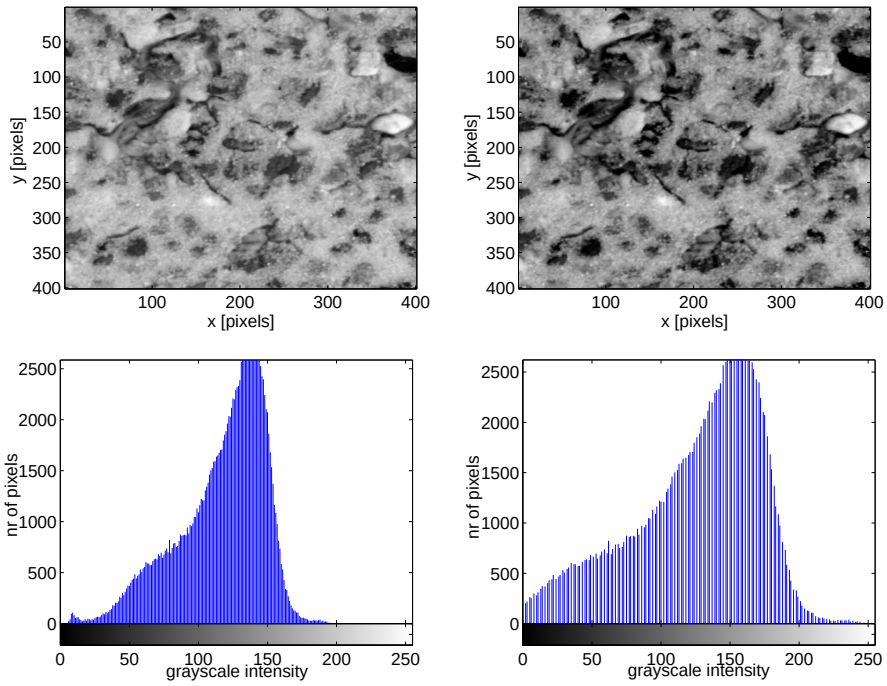

Figure A.2.1: Left column: Original image and image histogram showing the distribution of intensity values of the original image. Right: stretched image and stretched image histogram. ($Scale\,original\,images:\,111\,pixels = 10\,mm$)

Appendix B

Particle Tracking

B.1 Tracer Selection

The ideal tracer particles must exhibit the same behaviour as the rest of the fine fraction, but be distinct in appearance from both the fine fraction and the matrix. False positives are background areas that are classified as tracer particles; false negatives are tracer particles that are not identified as such.

A white sand that naturally contains a small fraction of dark particle, which can serve as tracer particles, is investigated. This requires a light matrix material, for which broken glass is used. The identification of the black particles is problematic due to shadows in the matrix. Grayscale stretching as described in Appendix A.2.1 does not improve this. There is no clear threshold between the colour of the tracer particles and the shadows, as illustrated in Figure B.1.1.

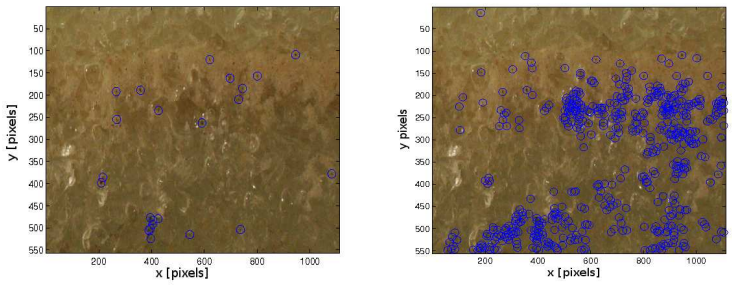

Figure B.1.1: The intensity of the tracer particles is similar to that of shadows in the matrix material. A higher threshold (left) results in many false negatives; a lower threshold (right) results in a high number of false positives. ($Scale: 230\,pixels = 10\,mm$)

Sand that is dyed green is considered as an alternative. The colour, not the brightness, is used to distinguish between the tracer particles and the background. Green sand particles are added to fine fractions of either white sand, or yellow/red sand, and combined with natural gravel (range of colours) or shattered glass as matrix materials. The colour difference is insufficient to identify the green particles unambiguously.

Shiny artificially coloured tracer particles stand out clearly when fully lit, and their colours are distinct from both the white sand and the gravel. Their shape differs from that of the fine fraction, they are flat with $D \approx 0.4\,mm$. They are made of aluminium foil; the unit weight of aluminium is slightly higher than that of the fine fraction, $\approx 27.0 - 27.5\,kNm^{-3}$. The particles are initially hydrophobic, this is remedied by pretreatment with ethanol. As these are the only tracer particles available that can be clearly identified, these particles are used in this work.

B.2 Tracer Identification

In a colour image, each pixel has a red (r), a green (g) and a blue (b) intensity value associated with it. To obtain a grayscale image, where each pixel is associated to one intensity value, the equation $g = 0.68r + 2$ is applied. This results in positive values for green tracer particles and negative values for most of the background, the negative values are set to zero. Positive values are linearly scaled over the pixel range $1 - 255$ to increase the contrast in the resulting image. In these images the tracer particles are the brightest objects and some matrix particles are still apparent.

A threshold is required to distinguish the remaining background from the tracer particles. This is particularly the case for the darker coarse grains. The value of the threshold is determined manually, and kept constant for the entire sequence of images.

Some matrix grains are above the threshold as shown in Figure 5.2.1, and increasing the threshold leads to false negatives. The spatial gradient of the pixel value in the pre-treated image is high at the edges of both matrix and tracer particles. Averaging the spatial gradient over an area with the size of the tracer particles, using a median filter, results in high values in the locations where tracer particles are present. These particles have a higher *edge/area* ratio than matrix grains. After this procedure, a second threshold can be used to eliminate the remaining matrix grains from the image.

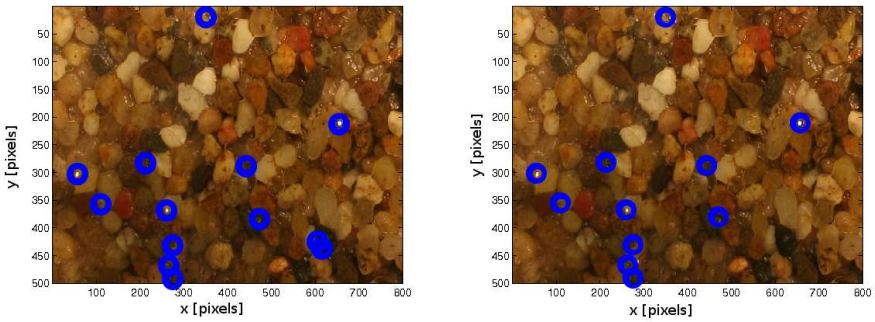

Figure B.2.1: When only colour is used to distinguish the tracer particles some matrix grains are falsely identified. This is the case at location (610, 450) in the left image. A matrix grain is identified as two tracer particles. In the right image an additional threshold, based on the gradient of the pixel value, is applied and these grains are no longer identified as tracer particles. ($Scale: 200\,pixels = 10\,mm$)

The use of different colours of tracer particles allows for an increase in the tracer seeding density. As shown in Figure B.2.2, blue particles can be distinguished from both matrix and green particles based on the blue and red intensity values.

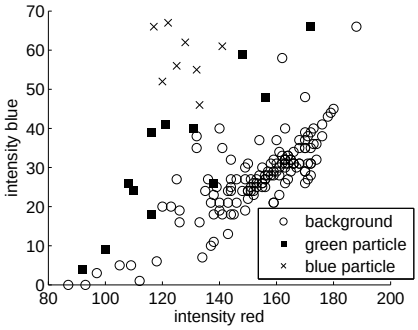

Figure B.2.2: Scatter plot of pixel values for green and blue tracer particles and background grains.

Appendix C

Image Subtraction

C.1 Threshold Determination

The main source of noise affecting image analysis using IS is due to variations in the illumination intensity. A threshold is required to remove this noise. Short wavelength noise due to image acquisition using the DSLR camera has little effect on the outcome of image analysis. For computational efficiency, no additional filters are applied to the original images to remove this noise.

The effect of variations in lighting intensity is investigated using the images acquired prior to the application of fluid flow. These contain no movement; thus the non zero values in the difference images can be assumed to be generated by variations in lighting intensity. This noise affects the entire image to the same extent, as shown in Figure C.1.1.

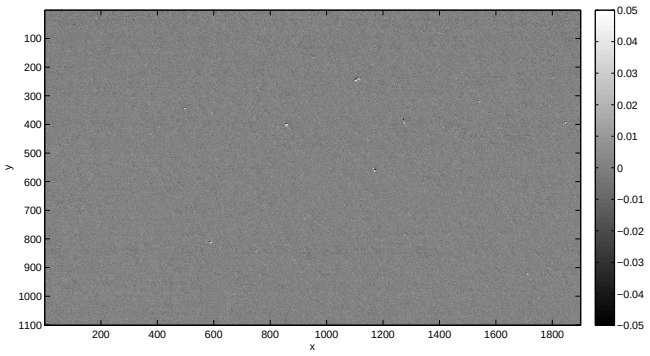

Figure C.1.1: Slight changes in illumination result in non zero values of the difference image; these appear to be uniformly distributed throughout the image. ($Scale: 111\,pixels = 10\,mm$)

As the illumination intensity varies during the experiment, the maximum variation of this must be determined using the entire sequence of images. The variation in illumination intensity causes stationary features, such as the scale bar attached to the outside of the model, to be visible in difference images. To ensure that the amount of movement that is determined using IS does not include artifacts due to variations in illumination intensity, a threshold is determined whereby the scale bar is not apparent in any of the difference images for the entire image sequence. The effect of this on a difference image where the illumination changed between two successive images is shown in Figure C.1.2.

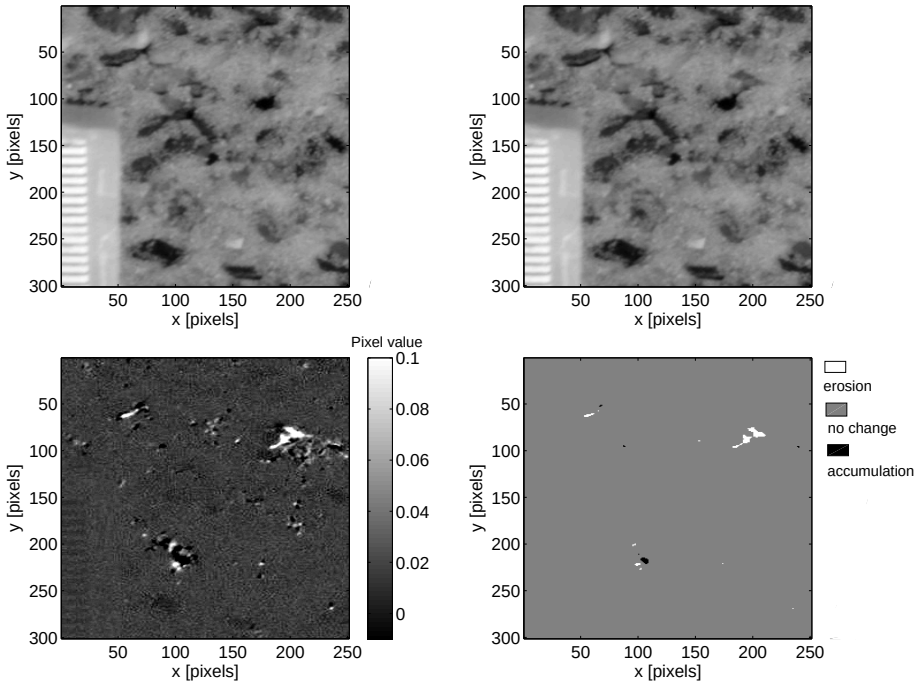

Figure C.1.2: Top row: two original images from test 7. Bottom row: The untreated difference image (left) contains artifacts due to changes in illumination. Applying a threshold of 0.1 removes these artifacts, leaving non zero values where fine particles have moved. ($Scale: 111\,pixels = 10\,mm$)

C.2 False Negatives

Part of the matrix has a grayscale intensity that is similar to that of the fine fraction. This can be seen in a histogram of the pixel values in Figure C.2.1. The two peaks correspond to intensities of the fine and the coarse fractions; the values in between can belong to either light matrix grains or shaded fine grains. The removal of fine grains from a light matrix grain results in an intensity difference that is below the threshold value that is determined in Appendix C.1. As a result of this, this area is indicated to display no change, referred to as a false negative.

To reduce the occurrence of false negatives, a distinction must be made between the light matrix grains and the fine particles. For this other properties than the grayscale intensity are considered.

The colour of an object, due to the specific combination of red, green and blue intensity values in a digital image, can be used to distinguish it from other objects. This is done in Chapter 5, for tracer particles. For the fine fraction used here, there is no characteristic ratio of colour intensities that can be used to distinguish the fine grains from the light and dark matrix grains, as shown in Figure C.2.2 The overlap of the fine grains with the coarse matrix grains indicates that the correlation between blue and green intensity values cannot be used to distinguish between the two materials.

Visual inspection of Figure C.2.3 suggests the light matrix grains have a more uniform, smooth, appearance than areas that contain a group of fine grains. This suggests that there is more variation in the pixel grayscale values in a region that contains multiple fine grains than in a region that contains a light matrix grain. Three different measures to quantify the variation in pixel grayscale values are investigated. Firstly, the image entropy, a measure of the randomness of pixel values. Secondly, the spatial gradient of the grayscale value, which is one of the characteristics used to distinguish between tracer particles and large matrix grains for PT in Appendix B.2. Thirdly, the standard deviation in the grayscale values over areas varying in dimension from 25 to 100 pixels. These measures all prove insufficient to distinguish between fine grains and light matrix grains.

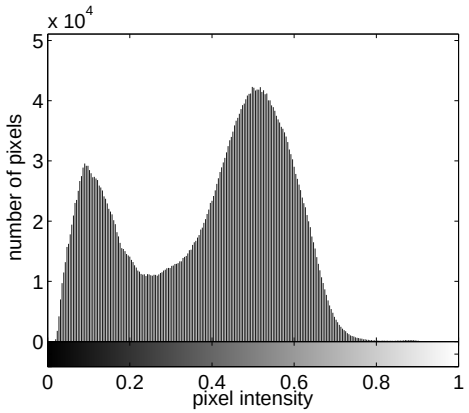

Figure C.2.1: The grayscale intensity distribution of the sample. The peaks correspond to the intensity of the fine grains (peak at 0.5) and the coarse grains (peak at 0.1) fractions. The intermediate values can belong to either light matrix or shaded fine grains.

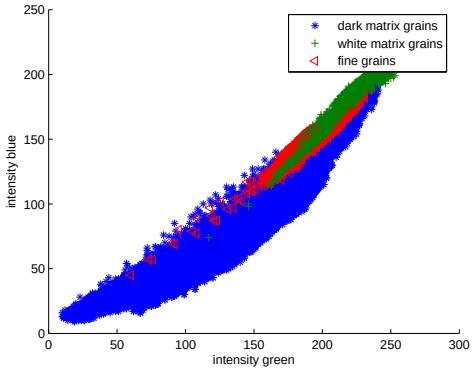

Figure C.2.2: Blue and green colour intensity of the coarse matrix grains and the fine grains.

Figure C.2.3: Fine fraction and the light matrix grains.

C.3 Quantification of Uncertainty

Manual inspection can be used to distinguish between the light matrix grains and fine fraction, however, manual inspection of all images is time intensive. Therefore, the total area of the image that does not indicate movement due to white matrix grains is quantified.

A summation of all the difference images that show motion is used to identify the areas where no motion is registered in tests 7 and 8. This is assigned a value 1 in a binary mask. This is applied to the final image of the sample, resulting in the image shown in Figure C.3.1. This contains: fines that have not moved, filter material below the sample, the particles composing the top load, the scale bar, and the desired light matrix grains. The light matrix grains are distinguished from the other material manually.

The area containing the top load particles and the filters is subtracted from the total area of the FOV, as no motion is possible there. However, in the area covered by the scale bar or by light matrix grains, movement of the fine particles is possible. For tests 7 and 8 this area consists of 1.37×10^5 pixels; it makes up 3.7% of the FOV.

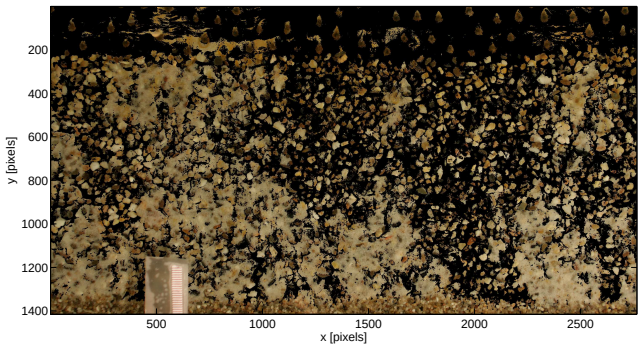

Figure C.3.1: Image area that shows no changes throughout tests 7 and 8. Black areas are those where motion is detected. ($Scale: 111\,pixels = 10\,mm$)

Appendix D

Data analysis

D.1 Connectivity of Flow Paths

In test 7, the areas that indicate high activity do not form connected flow paths in the FOV. Figure D.1.1 shows all the areas that display a high amount of activity, as well as those areas where the contrast is below the threshold and that are therefore uncertain. This addition does not result in connected vertical pathways. This suggests that the flow paths transporting fines have a component in the third dimension. This is expected as porosity at the wall of the sample is less than 1.

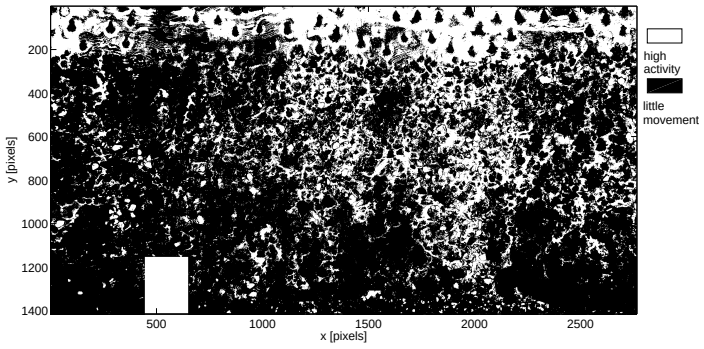

Figure D.1.1: Uncertain areas are assumed to contain high activity, in combination with the areas that are observed to have a high activity few connected paths are present in the plane of view. This indicates particle transport has a component in the 3^{rd} dimension. ($Scale: 111\,pixels = 10\,mm$)

D.2 Total Change During Test 7

Figure D.2.1 shows the total change in the sample during the 6 stages of test 7. In the first stage, the application of flow leads to erosion throughout the sample. In the next stage, flow is at constant hydraulic head, and there is significant erosion of fines. This is more concentrated in specific areas than the movement in the first stage.

The subsequent increments of the hydraulic head, in stages 3 and 5, lead to much less movement. During the stages of constant head following these, erosion occurs both in larger connected patches and scattered through the sample. The periods of constant hydraulic head last $590\,s$ each, whereas the increments are applied over $10\,s$. This can account for a greater change occurring during the constant head stages 4 and 6 than during stages 3 and 5 when the head is increased.

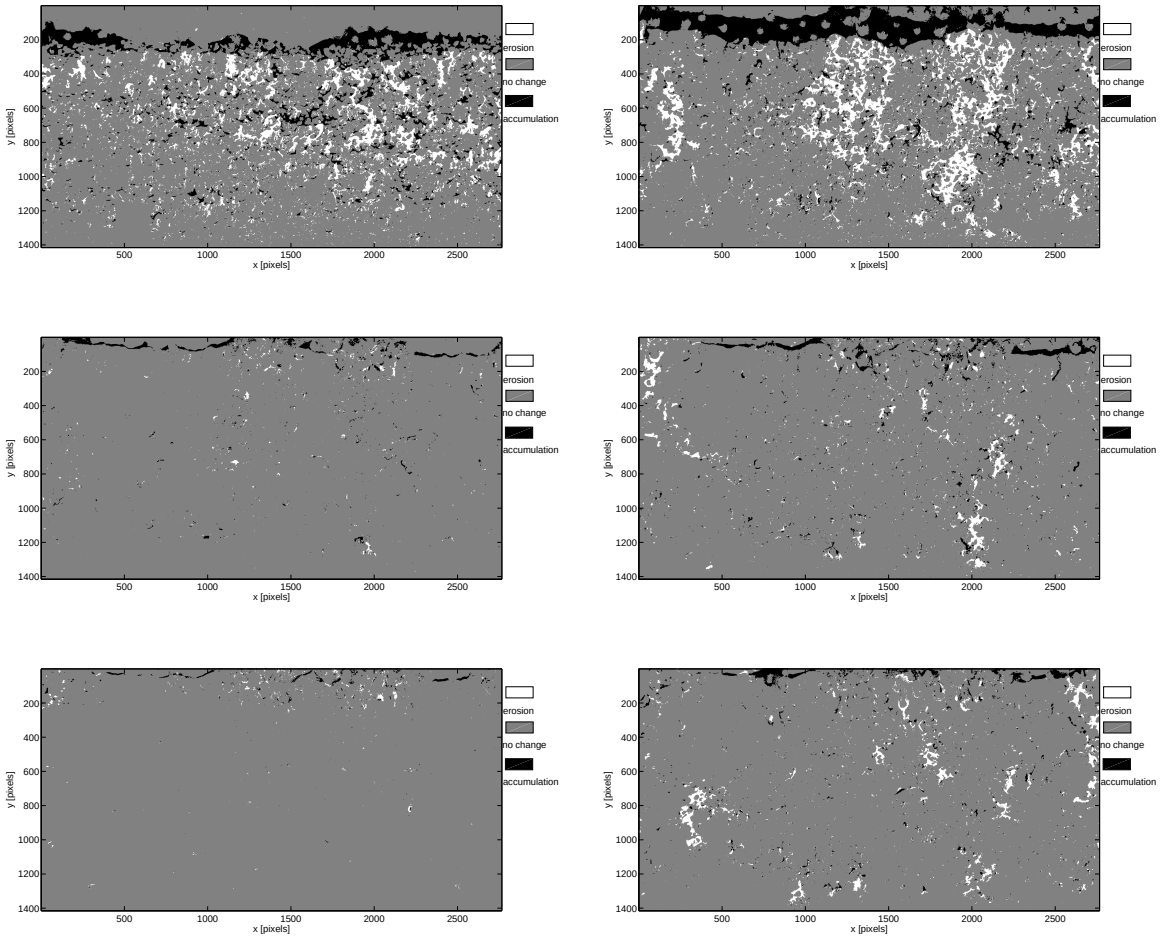

Figure D.2.1: Total change in the sample during and after the application of the hydraulic head in 3 steps during test 7. Left column: the difference over the period in which the head is raised ($10\,s$). Right column: the difference over the ensuing periods of constant head ($590\,s$). ($Scale: 111\,pixels = 10\,mm$)

D.3 High Spatial Resolution IS

Zooming in on the sample, in test 3, allows the study of individual fine grains on the pore scale. The FOV is $10 \times 14\,mm$; fine particles are represented by approximately 40 pixels. The sequence of images acquired whilst the hydraulic head is applied to the sample for $10\,s$ is analysed and the results are shown in Figure D.3.1.

A summation 10 difference images that indicate motion shows that motion is concentrated in one area. This suggests that preferential flow paths exist also on the pore scale. The majority of the movement appears to be around the edge of a matrix grain in a region that contains some free pore space. Areas where the concentration of fines is very high, such as the left bottom of the image, display little movement.

The total change in the fines content during this time period indicates that erosion and accumulation predominantly occur near the preferential flow path. Near the path, large patches indicate erosion or accumulation; in the remainder of the image, smaller speckles of erosion and accumulation occur.

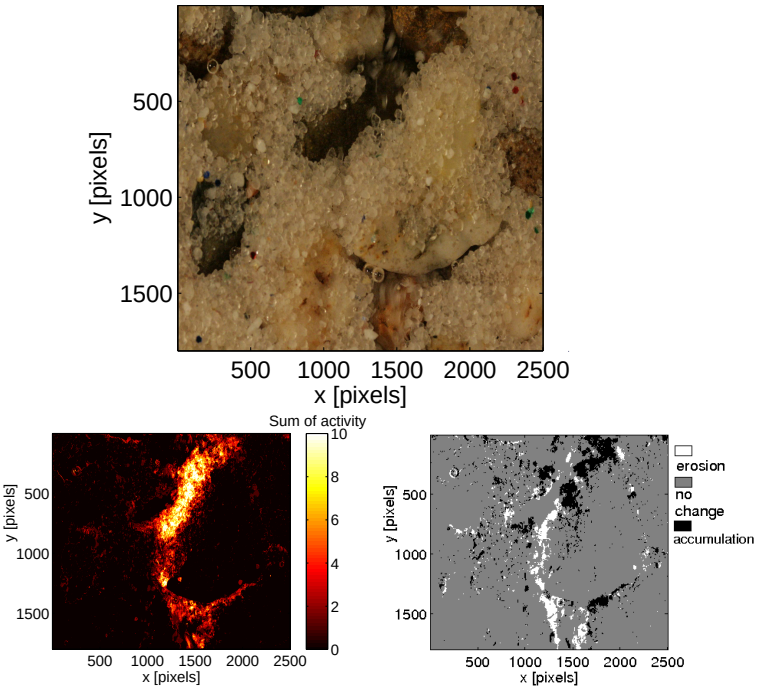

Figure D.3.1: Analysis of a sequence of images where the flow rate is applied to the sample using a FOV is $14 * 10\,mm$. Top: original image at $t = 0$. Bottom left: the summation of 10 difference images that indicate motion. Bottom right the total change over the $10\,s$ during which the flow is applied. ($Scale: 201\,pixels = 10\,mm$)